Crystal structure of human RhoA complexed with a GTP analogue

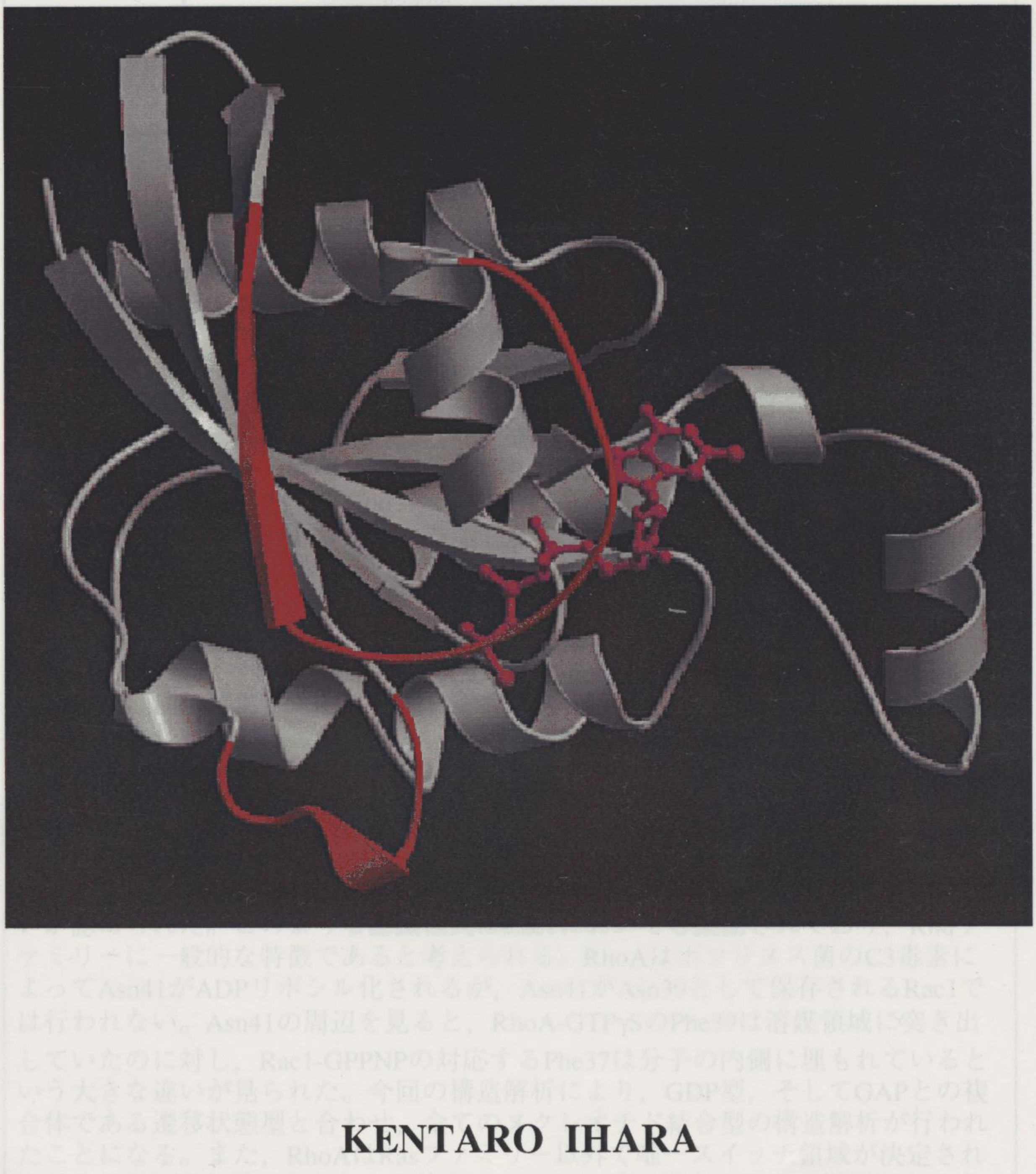

KENTARO IHARA

バイオサイエンス研究科　博士論文要旨

所　属 （主指導教官）	バイオサイエンス研究科　生体高分子構造学講座（箱嶋　敏雄）		
氏　名	伊原　健太郎	提　出	平成１１年　１月　７日
題　目	Crystal structure of human RhoA complexed with a GTP analogue （活性型ヒトRhoA-GTPアナログ複合体の結晶構造）		

要旨

低分子量G蛋白質は分子量2万から3万のGTP結合蛋白質の総称であり，アミノ酸配列の類似性からRas, Rhoなどの数種類のファミリーに分類される。いずれもMg^{2+}の存在下でGTPとGDPに強く結合し，GTP結合型とGDP結合型の間の大きなコンフォメーション変化を利用して異なった標的蛋白質を認識する。Rhoは主に細胞骨格や細胞接着に関わる。我々はRhoファミリーの構造的特徴を明らかにし，標的特異性の決定機構を解明するためにRhoAとGTPアナログであるGTPγSとの複合体の結晶構造解析を行った。初期位相の決定はH-Ras-GPPNPを用いた分子置換法によって行い，構造の精密化により最終的に分解能2.4 Å, R=19.5 %, R$_{\mathrm{free}}$=26.8 %の構造を得た。Rhoファミリーの蛋白質はRasファミリーと比較して13アミノ酸残基の挿入があるが，この部位が1つのαヘリックスを形成することが明らかとなった。H-Ras-GTPの構造との比較により，Switch IとSwitch II，及びその中間の逆平行βシートの3箇所に大きな構造の違いが見られ，これらの領域がRhoファミリーとRasファミリーの標的特異性を決定することが示された。また，RhoA-GDPとの構造比較によって，RhoAのSwitch IはAsp28からAla44，Switch IIはGly62からLeu69であることが判明し，スイッチ領域以外にはほとんど構造の変化が見られなかった。RhoAとRac1はそれぞれRhoサブファミリーとRacサブファミリーに属し，アミノ酸の同一性が56 %である。Rac1-GPPNPとの構造の比較の結果，Switch I付近(Val33-Ile46)と13アミノ酸残基の挿入領域付近(Asn123-Gln136)に比較的大きな主鎖の動きが集中していた。これらの領域はRac1の標的蛋白質であるp67phoxの認識領域とも一致することから，標的特異性への関与が考えられる。GTPの認識はH-Rasと類似していたが，糖と塩基の2つの水分子を介した認識に違いが認められた。このような認識様式はRac1においても観測されており，Rhoファミリーに一般的な特徴であると考えられる。RhoAはボツリヌス菌のC3毒素によってAsn41がADPリボシル化されるが，Asn41がAsn39として保存されるRac1では行われない。Asn41の周辺を見ると，RhoA-GTPγSのPhe39は溶媒領域に突き出していたのに対し，Rac1-GPPNPの対応するPhe37は分子の内側に埋もれているという大きな違いが見られた。今回の構造解析により，GDP型，そしてGAPとの複合体である遷移状態型と合わせ，全てのヌクレオチド結合型の構造解析が行われたことになる。また，RhoAはRasファミリー以外で唯一スイッチ領域が決定された低分子量G蛋白質でもあり，今後のスイッチングに関する研究の指標になるものと思われる。

Crystal structure of human RhoA complexed with a GTP analogue

（活性型ヒトRhoA-GTPアナログ複合体の結晶構造）

伊原　健太郎
奈良先端科学技術大学院大学
バイオサイエンス研究科　生体高分子構造学講座
（箱嶋　敏雄　教授）

平成１１年　１月　７日提出

Contents

Introduction 3

Materials and methods 10

Preparation and crystallization of RhoA^{V14} 10

Data collection and structure determination 11

Structure refinement 12

Results 24

Overall structure 24

Insertion regions 25

Phosphate-binding loop 27

Switch I 27

Strand B2 and B3 28

Switch II 29

Magnesium ion binding 30

Guanosine nucleotide binding 30

Triphosphate binding 31

Putative nucleophilic water molecule 32

Discussion 48

Modification sites by bacterial toxins 48

GTP/GDP switching and effector binding 50

GEF and GDS binding 52

GDI binding 53

Effects of the γ-sulfur atom and the G14V mutation on the GTPase activity 53

Conclusion 61

Acknowledgements 62

References 63

Introduction

Based on sequence and apparent functional homology, the superfamily of Ras-related small guanosine triphosphatase (GTPase) proteins can be subdivided into the Ras, Rho, Ran, Rab, Arf, Sar and Rad families, with more families still to be defined (Wittinghofer and Nassar, 1996). Rho is a small GTPase that was first purified from mammalian tissue membrane (Yamamoto *et al.*, 1988) and cytosol (Morii *et al.*, 1988) fractions and was identified as the gene product of the *ras* homologue gene, *rho* (Madaule *et al.*, 1985). Rho has three mammalian isoforms, RhoA, RhoB, and RhoC, that exhibit high sequence homology with 83 % identities (Symons, 1996). Rho cycles between GTP-bound and GDP-bound forms in a similar manner as Ras and other small GTPases. The level of the active GTP-bound form is regulated by its own guanine nucleotide dissociation inhibitor (GDI), guanine nucleotide exchange factor (GEF), and GTPase activating protein (GAP). The interconversion between the GTP-bound and GDP-bound forms allows Rho to act as a molecular switch that regulates intercellular signaling pathway (Fig. 1). Rho is implicated in the cytoskeletal responses to extracellular signals including lysophosphatidic acid and certain growth factors, which result in the formation of stress fibers and focal adhesion (Machesky *et al.*, 1996; Narumiya *et al.*, 1996; Takai *et al.*, 1995). Recent isolation and characterization of putative target proteins for Rho from the bovine brain (Kimura *et al.*, 1996; Matsui *et al.*, 1996) have led to a possible mechanism by which Rho regulates cytokinesis, cell motility, or smooth muscle contraction (Amano *et al.*, 1996a; Amano *et al.*, 1997; Chihara *et al.*, 1997). These proteins contain the myosin-binding subunit (MBS) made up of myosin phosphatase and novel serine/threonine kinase, Rho-kinase, that has been shown to phosphorylate MBS to inactivate myosin phosphatase and also to phosphorylate myosin light-chain (MLC). Accumulation of phosphorylated MLC induces a conformational change in myosin II that increases its interaction with actin and enables the formation of myosin filaments (Tan *et al.*, 1992). This myosin II activation promotes neurite retraction in N1E-115 neuroblastoma cells (Amano *et al.*, 1998).

Rho-kinase also phosphorylates the C-terminal threonines of ezrin/radixin/moesin (ERM) proteins and regulates their head-to-tail association (Matsui *et al.*, 1998). Rho-kinase is identical to ROK from the rat brain (Leung *et al.*, 1996) and p160ROCK from human megakaryocytic leukemia cells (Ishizaki *et al.*, 1996; Ishizaki *et al.*, 1997), which are members of a growing family of serine/threonine protein kinases that include myotonic dystrophy kinase. Recently, p160ROCK mediates RhoA activation pathway regulating focal adhesion and stress fiber formation via Na-H exchanger, NHE1 (Tominaga *et al.*, 1998). Other target proteins for Rho contain protein kinase N (PKN) (Amano *et al.*, 1996b; Watanabe *et al.*, 1996), Rhophilin (Watanabe *et al.*, 1996), Rhotekin (Reid *et al.*, 1996), and Citron (Madule *et al.*, 1995). It has been shown that Citron localizes at the cleavage furrow and midbody of HeLa cells with RhoA to regulates cytokinesis during mitosis (Madule *et al.*, 1998). Further signaling pathways for actin polymerization have appeared to involve phosphatidylinositol (PtdIns) 4-phosphate 5-kinase (Ren *et al.*, 1996) and p140mDia (Watanabe *et al.*, 1997), as downstream effectors.

Rho has two related small GTPases, Rac and Cdc42, that are also involved in regulating the organization of the actin cytoskeleton, whereas the cell morphological effects induced by these GTPases are clearly different in appearance (Fig. 2). Rac regulates lamellipodium formation and membrane ruffling, and Cdc42 regulates filopodium formation. Rac is also known to be involved in the activation of NADPH oxidase in phagocytes (Abo *et al.*, 1991). Rac has two mammalian isoforms, Rac1 and Rac2, that exhibit a high sequence homology with 90 % identities. Rac and Cdc42 also share a significant homology with 68 % identities and, actually, bind to some common target proteins for activation. Rho, however, exhibits a relatively low similarity to Rac and Cdc42. These differences in similarity are thought to be essential for the activation of several downstream target proteins of each small GTPase, although we do not yet understand the molecular basis of the specificities. Recent studies showed that these small GTPases regulate transcriptional regulation through such as serum response ractor (SRF) or nuclear transctiption factor-κB (NF-κB) (Hill *et al.*, 1995; Perona *et al.*, 1997). Based on these differences, RhoA, RhoB, and RhoC are hereafter referred to as the Rho subfamily, and Rac1, Rac2, and Cdc42 as the Rac subfamily. The Rho-binding domains of the target proteins consist of less than 100 residues and have been classified into at least two motifs (Matsui *et al.*, 1996; Fujisawa *et al.*, 1996; Fujisawa *et al.*, 1997; Van Aelst and D'Souza-Schorey, 1997). The class 1 of the Rho-binding motif is characterized as a polybasic region followed by a leucine-zipper-like motif and is found in PKN, PRK2, Rhophilin, and Rhotekin. Rho-kinase/ROKα, p160ROCK/ROKβ/ROCK-II and Citron make up another class of the Rho-binding motif, class 2, that has a putative coiled-coil motif located at the C-terminus of the segment that is similar to myosin rod. Some proteins such as MBS or p140mDia are not yet classified. It is of considerable interest that these sequences of the Rho-binding domains have no similarity to the binding domain of an activated Cdc42Hs-associated kinase (ACK) (Manser *et al.*, 1993), a p21(Cdc42/Rac1)-activated protein kinase (PAK) (Manser *et al.*, 1994), or the Ras-binding domain of Raf-1 (Fabian *et al.*, 1994).

Rho and the related small GTPases are the most common targets for bacterial toxins and are of major importance for the entry of bacteria into mammalian host cells. It is well known that various bacterial toxins can modify Rho by ADP-ribosylation, glucosylation, and deamidation. These toxins are classified into three families, C3-like exoenzymes such as *Clostridium botulinum* C3 ADP-ribosyltransferase, large clostridial cytotoxins such as *Clostridium difficile* toxins A, and Rho-activating toxins such as *Escherichia coli* cytotoxic necrotizing factors (CNFs) (Aktories, 1997). The C3-like exoenzymes act on members of the Rho subfamily, but most of the large clostridial cytotoxins inactivate all members of the Rho family. The Rho-activating toxins activate members of the Rho subfamily and Cdc42. No activity for Ras, Rap, and Ran has been reported for the bacterial toxins of these three families, but *Clostridium sordelli* HT, one of the large clostridial cytotoxin, is known to inactivate Ras and Rap. There is no interpretation for these emerging differences in the specificity of the small GTPases. Hence, it becomes essential to examine the three-dimensional structures of Rho to understand how their interactions with the target proteins control the various signaling processes and how the modification by bacterial toxins change the activities of their target GTPases for bacterial invasion. We report here the crystal structure of recombinant human RhoA, which is dominantly activated with substitution of Gly14 by valine (RhoA^{V14}) (Fig. 3), complexed with GTP analogue, guanosine 5'-3-*O*-(thio)-triphosphate (GTPγS), and we compare it with the structures of H-Ras, RhoA-GDP and other related GTPases.

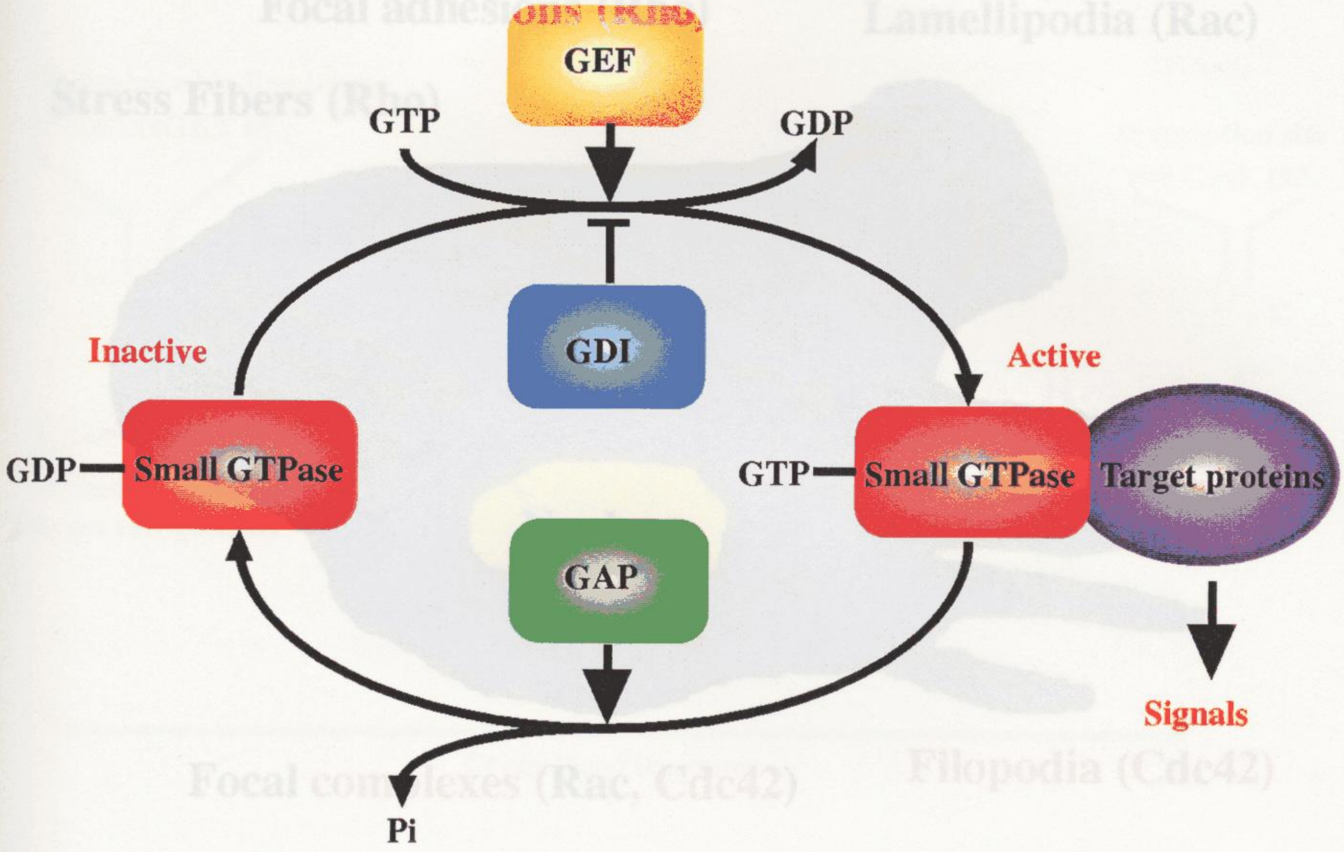
GEF
GTP
GDP
GDI
Inactive
Active
GDP
Small GTPase
GTP
Small GTPase
Target proteins
GAP
Signals
Pi

Fig. 1. The small GTPase cycle and its regulations.
Small GTPases cycle between GTP-bound and GDP-bound forms. Usually, this cycle is regulated by GDIs, GEFs, and GAPs. The GTP-bound form can interact with their downstream target molecules.

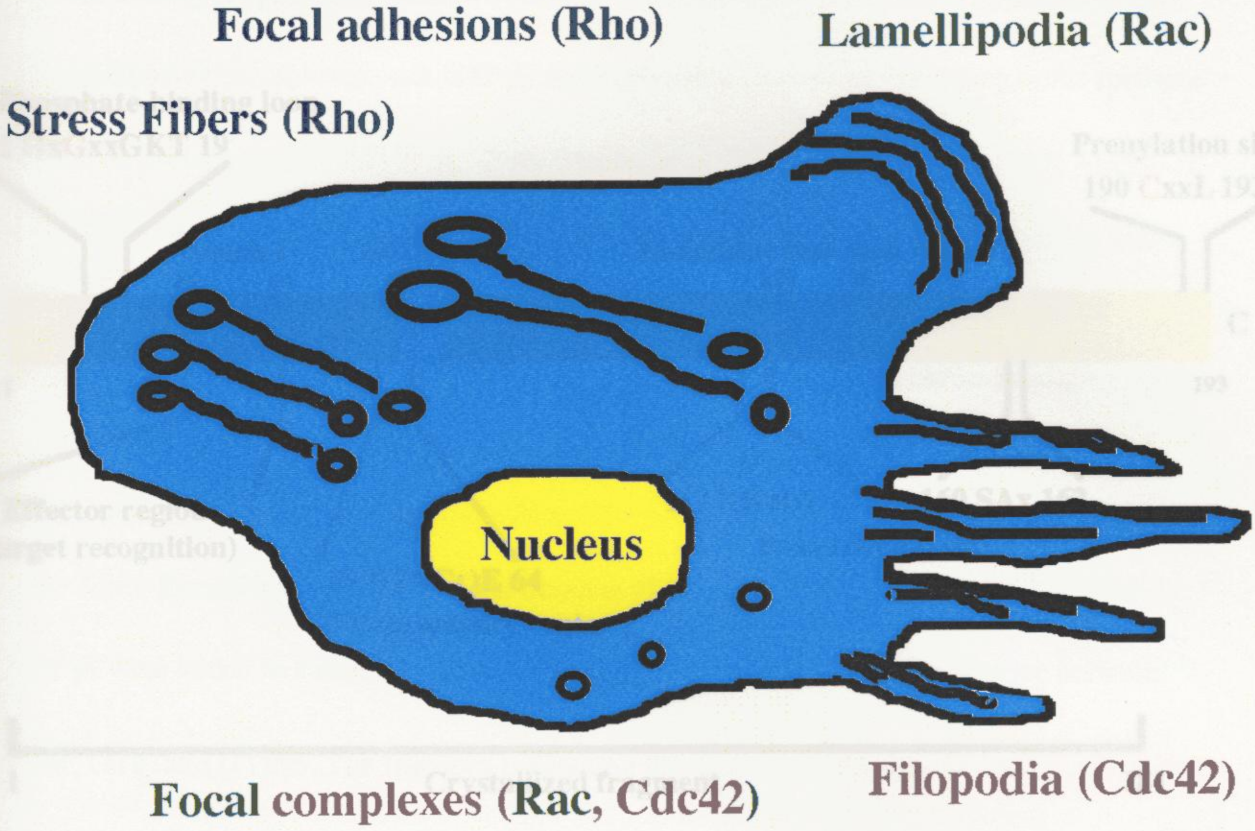
Focal adhesions (Rho)
Lamellipodia (Rac)
Stress Fibers (Rho)
Nucleus
Focal complexes (Rac, Cdc42)
Filopodia (Cdc42)

Fig. 2. Cell morphologies induced by the Rho family small GTPases.
The Rho family small GTPases are involved in regulating the organization of the actin cytoskeleton and the cell adhesion molecules. The Rho subfamily and the Rac subfamily show different cell morphologies: RhoA, RhoB, and RhoC regulate the formation of focal adhesions and stress fibers; Rac1, Rac2, and Cdc42 regulate the formation of lamellipodia, filopodia and focal complexes.

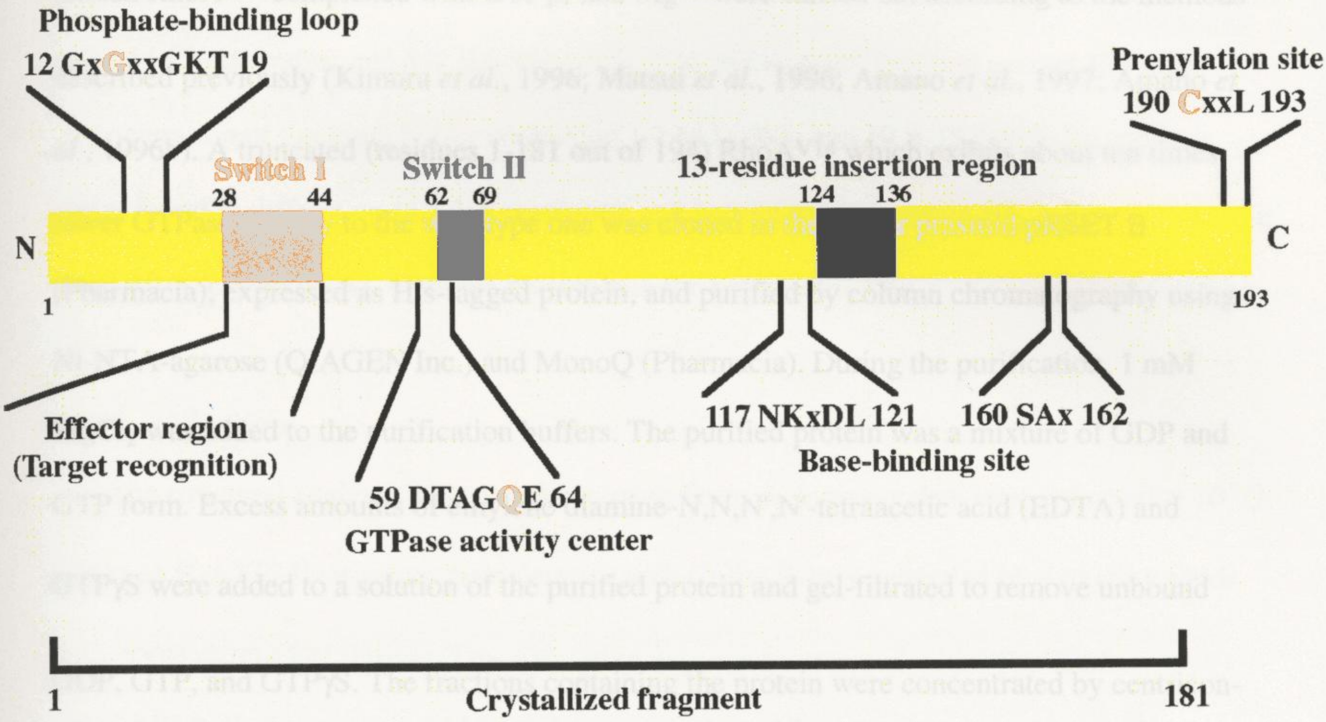
Phosphate-binding loop
12 GxGxxGKT 19
Switch I
28
44
Switch II
62
69
13-residue insertion region
124
136
Prenylation site
190 CxxL 193
N
C
1
193
Effector region
(Target recognition)
59 DTAGQE 64
GTPase activity center
117 NKxDL 121
160 SAx 162
Base-binding site
1
Crystallized fragment
181

Fig. 3. Structural features of RhoA.

RhoA is composed by 193 residues and has a 13-residue insertion region which is unique to the Rho family GTPases. The other consensus regions are common to all small GTPases. RhoA has a prenylation site at its C-terminus. This region was omitted from the fragment for crystallization because of its flexibility. It is known that the mutations to Gly14 and Qln63 remarkably reduse GTPase activity. In this study, Gly14 is mutated to Val.

Materials and methods

Preparation and crystallization of RhoA^{V14}

The cloning, expression, and purification of the dominantly active form of recombinant human RhoA^{V14} complexed with GTPγS and Mg^{2+} were carried out according to the methods described previously (Kimura *et al.*, 1996; Matsui *et al.*, 1996; Amano *et al.*, 1997; Amano *et al.*, 1996b). A truncated (residues 1-181 out of 194) RhoA^{V14} which exibits about ten times lower GTPase activity to the wild type one was cloned in the vector prasmid pRSET B (Pharmacia), expressed as His-tagged protein, and purified by column chromatography using Ni-NTA-agarose (QIAGEN Inc.) and MonoQ (Pharmacia). During the purification, 1 mM $MgCl_2$ was added to the purification buffers. The purified protein was a mixture of GDP and GTP form. Excess amounts of ethylene diamine-N,N,N',N'-tetraacetic acid (EDTA) and GTPγS were added to a solution of the purified protein and gel-filtrated to remove unbound GDP, GTP, and GTPγS. The fractions containing the protein were concentrated by centricon-10 (Amicon Inc.) for crystallization. The resulting sample, used in this study, is verified with matrix-assisted laser desorption/ionization time-of-flight mass spectroscopy (MALDI-TOF MS) (LMS-ELITE, PerSeptive Inc.) and N-terminal analysis (M492, Applied Biosystems), which showed the spontaneous truncation of N-terminal His-tag during the preparation and one additional serine residue at the N-terminus.

Crystals were obtained at 4 °C by the hanging-drop vapor diffusion method from solutions containing 10 mg/ml RhoA^{V14}-GTPγS, 50 mM Tris-HCl buffer, pH 8.5, 10 % PEG8000, 7.5 % 1,4-dioxane equilibrated against 100 mM concentration of the same buffer containing 20 % PEG8000 and 15 % 1,4-dioxane. Plate-like crystals (Form A) grew within a few days and were found to diffract up to 2.4 Å resolution. The crystals belong to space group $P2_12_12$ (a = 62.02 Å, b = 74.78 Å, c = 50.52 Å), with one molecule in the asymmetric unit (see below). Another hexagonal crystal form (Form B) was also obtained from solutions containing 10 mg/ml RhoA^{V14}-GTPγS, 50 mM sodium acetate buffer, pH 4.6, 10 % 2-propanol equilibrated against 100 mM of the same buffer containing 20 % 2-propanol. Crystals had hexagonal or trigonal lattice parameters with a rather long c axis (a = b = 60.80 Å, c = 214.56 Å) and diffracted at 3.0 Å. RhoA^{V14}-GDP crystals were also obtained from solutions containg 3 mg/ml RhoA^{V14}-GDP, 50 mM Citrate buffer, pH 5.0, 0.6 M Li_2SO_4, 5 % PEG400 equilibrated against 100 mM concentration of the same buffer containing 1.2 M Li_2SO_4 and 10 % PEG400. The crystals were found to diffract up to 2.2 Å resolution and belong to space group $P4_32_12$ (a = 91.40 Å, b = 91.40 Å, c = 56.62 Å), with one molecule in the asymmetric unit.

Data collection

The structural analysis was carried out using Form A. Intensity data were collected at 10 °C using an R-AXIS IIc imaging plate detector with CuKα X-rays generated by a rotating anode RU-300H (RIGAKU, Japan). The diffraction data were processed with PROCESS (RIGAKU). Each intensity, $I(hkl)$, of data was evaluated from the imaging plates and transformed to the amplitude of structure factor, $F(hkl)$. We observed 61,579 reflections containg 8,683 unique reflections with a completeness of 89.3 % and R_{merge}=8.75 %. The reliability of the data, R_{merge}, is defined by,

$$R_{merge} = \frac{\Sigma \left| I_i(hkl) - \langle I(hkl) \rangle \right|}{\Sigma I_i(hkl)},$$

where $I_i(hkl)$ is the i-th measurement and $<I(hkl)>$ is the mean of the measurements of reflection hkl. The typical value of R_{merge} is under 10 %.

An estimation of the number of molecules per unit cell, Z, can be made by a V_m value which is the ratio of the unit cell volume and the molecular weight (Matthews, 1968). The V_m value is given by,

$$V_{\mathrm{m}} = \frac{V_{\mathrm{cell}}}{\mathrm{M_W Z}},$$

where V_{cell} is the volume of the unit cell and $\mathrm{M_w}$ is the molecular weight of the protein. V_{m} values usually range between 1.7 and 3.5 Å3/Da for protein crystals. The RhoA$^{\mathrm{V14}}$-GTPγS crystal was estimated to contain one molecule in the asymmetric unit (Z=4) with a V_{m} value of 2.77 Å3/Da. The solvent content of the crystal, V_{solv}, is calculated from V_{m} values by,

$$V_{\mathrm{solv}} = 1 - \frac{1.23}{V_{\mathrm{m}}},$$

and this scheme gave 0.56 for the RhoA$^{\mathrm{V14}}$-GTPγS crystal. A summary of the crystal data is given in Table 1, and a summary of the data processing statistics is given in Table 2.

Structure determination and refinement

Molecular replacement

The electron density $\rho(xyx)$ of the crystal is calculated with structure factors, $\mathbf{F}(hkl)$, by,

$$\rho(xyz) = \frac{1}{\mathrm{V}} \Sigma\Sigma\Sigma \mathbf{F}(hkl) \exp[-2\pi i(hx + ky + lz)],$$

$$\mathbf{F}(hkl) = F(hkl) \exp[i\alpha(hkl)],$$

and,

$$F^2(hkl) = I(hkl),$$

where x, y, and z are relative coordinates in the real space unit cell, and h, k, and l are the reciprocal lattice points. The X-ray diffraction experiments give only the amplitudes of structure factors, $F(hkl)$. To obtain the electron density, the phase angles of structure factors, $\alpha(hkl)$, are needed. There are several techniques to obtain protein crystal phases using heavy atom isomorphous replacement method, anomalous scattering method, or molecular replacement method. The molecular replacement method can be applied if the structure of the protein or homologous proteins have already established. Without phase angles of structure factors, the Patterson function, *P(uvw)*, can be calculated by Fourier summation with intensities as coefficients,

$$P(uvw) = \frac{1}{V} \Sigma F^2(hkl) \cos[2\pi(hu + kv + lw)],$$

where *u, v,* and *w* are relative coordinates in the Patterson cell, which has dimensions identical to the real cell. The Patterson function can alternatively be written as,

$$P(\mathbf{u}) = {}_{\text{cell}}\rho(\mathbf{x})\rho(\mathbf{x}+\mathbf{u})dv.$$

This equation means that the Patterson function will have a large value only if the positions **x** and **x+u** both represent atomic positions, that is when **u** is an interatomic vector. The Patterson function, therefore, represents a map of the interatomic vectors including self-vectors at the origin. If a real unit cell contains N atoms, the corresponding Patterson map will show N(N-1) peaks around the origin. A large number of N such as proteins give too many peaks to interpret, so it is impossible to determine the whole structure from the Patterson function. However, molecules haning a similar shape show similar Patterson maps and the known protein molecular structure from its crystalline arrangement can be transfered to the crystal of the protein for which the structure is not yet known by fitting the Patterson functions together. This is the molecular replacement method and involves two steps: rotation and translation (Rossmann and Blow, 1962). At first rotation matrix, [C], is needed to determine to maximize an overlap function *R*(C) defined as,

$$R(\mathrm{C}) = {}_{U}P(\mathbf{u})P_{\text{model}}([\mathrm{C}]\mathbf{u})d\mathbf{u}.$$

$P(\mathbf{u})$ is the Patterson function of unknown structure, $P_{\text{model}}([\mathrm{C}]\mathbf{u})$ is rotated Patterson function of the model Patterson function $P_{\text{model}}(\mathbf{u})$ by matrix [C], and *U* is the volume in the Patterson map where the self-Patterson peaks are located. Correct matrix [C] will give a maximum value.

In the next step, translation vector, **m**, can be determined to maximize another overlap function $T_2(\mathbf{m})$, a translation function (Crowther and Blow, 1967; Crowther, 1972), defined as,

$$T_2(\mathbf{m}) = {}_V P(\mathbf{u}) P_{\text{model}}(\mathbf{m},\ \mathbf{u}) d\mathbf{u}.$$

It results in peaks corresponding to all possible intermolecular vectors in the unknown stucture. The model structure contains the same number of molecules as the unknown crystal structure has in its unit cell. $P_{\text{model}}(\mathbf{m}, \mathbf{u})$ is cross-Patterson function between the all molecules existing in the unit cell. $P_{\text{model}}(\mathbf{u})$ is created from the model structure by rotation matrix [C], and **m** is the position vector of one of the molecules existing in the unit cell. The positions of the other molecules are calculated by crystallographic symmetry operations to **m**.

Reliability of the solutions are judged by calculating an *R*-factor, *R*, or the correlation coefficient, *C*, defined as,

$$R = \frac{\Sigma \,||\mathbf{F}(\text{obs})| - k|\mathbf{F}(\text{calc})||}{\Sigma\, |\mathbf{F}(\text{obs})|},$$

$$k = \frac{\Sigma\, |\mathbf{F}(\text{obs})|\ |\mathbf{F}(\text{calc})|}{\Sigma(|\mathbf{F}(\text{calc})|)^2},$$

and,

$$C = \frac{\Sigma(|\mathbf{F}(\text{obs})|^2 - \overline{|\mathbf{F}(\text{obs})|^2})(|\mathbf{F}(\text{calc})|^2 - \overline{|\mathbf{F}(\text{calc})|^2})}{\left[\Sigma(|\mathbf{F}(\text{obs})|^2 - \overline{|\mathbf{F}(\text{obs})|^2})^2 \Sigma(|\mathbf{F}(\text{calc})|^2 - \overline{|\mathbf{F}(\text{calc})|^2})^2\right]^{1/2}}.$$

Both schemes gave the agreement index between calculated structure factors, **F**(calc), and observed structure factors, **F**(obs). The *R*-factor includes a scale factor *k* for the intensities, but not for the correlation coeficient and is scaling insensitive, so the correlation coeficient has an advantage over The *R*-factor. In the refinement, The *R*-factor has to be minimized and the correlation coeficient has to be maximized.

The initial phases were calculated by molecular replacement with the program AMoRe

(Navaza, 1994) using a search model based on the structure of human H-Ras (Protein Data Bank code 5P21, Brookhaven National Laboratory), with which RhoA shares a 27.5 % identity. At the same time, several searches with a polyalanine model were performed with X-PLOR (Brünger *et al.*, 1990). After calculations of possible four space groups, $P222$, $P222_1$, $P2_12_12$, $P2_12_12_1$, both methods gave the highest correlation coeficient and the lowest *R*-factor when the crystal belong to $P2_12_12$. A summary of the solutions of rotation and translation function by AMoRe is given in Table 3.

Model building and refinement

The model obtained was divided into the secondary structure elements, and again, rigid body refinements were performed with X-PLOR. Rigid body refinement is the process of refining the positions of rigid groups of atoms against the observed amplitudes and this is often done as a first step in a refinement procedure after the molecular replacement procedure has given starting values for the position and orientation of the model. The protein model is devided into one or more groups and each group are refined the six parameters, three rotations and three translations, according to the *R*-factors or the correlation coefficients described above. Followed by rigid body refinements, solvent flattening/histogram matching with the program DM (Cowtan and Main, 1996) were also performed with the solvent content of 56 %. Solvent flattening is based on the assumption that a structure factor from crystal is a summation of that from protein and solvent regions,

$$\mathbf{F}_{\mathrm{crystal}} = \mathbf{F}_{\mathrm{protein}} + \mathbf{F}_{\mathrm{solvent}},$$

and one can get improved $\mathbf{F}_{\mathrm{crystal}}$ by refining not only $\mathbf{F}_{\mathrm{protein}}$ but also $\mathbf{F}_{\mathrm{solvent}}$. In the highly refined protein crystal structures, it is known that the electron density map of the solvent region is rather flat compared to protein region. Except around the protein, the solvent has a dynamic nature and its time-averaged electron density has a low constant value. If the protein region can be identified, the rest density should be set to a low constant value. After solvent flattening, new structure factor amplitudes and phases are calculated using Fourier transform of density and the next electron density map is calculated with these improved phase angles. In this study, the molecular envelope around the protein was defined by visual inspection from the preliminary electron density map using the model phases. Histogram matching is another method which modifies the electron density map, and based on the empirical fact that electron density maps of well-refined proteins have similar histograms to each other when they have the same resolution range and similar solvent contents. To make the histogram, at first the grid points of the electron density map are grouped by their density sizes into the same interval ranges and, next, the number in the same range is counted. Obtained histogram is fitted onto the ideal histogram which is calculated under the same resolution range and solvent content. These modified electron densities are put back to the grid points, and new structure factors are calculated. In this way, four regions of insertions and deletions were inspected on the resulting 2Fo-Fc map that was generated with the program O (Jones *et al.*, 1991). 2Fo-Fc map is the calculated electron density using 2|**F**(obs)| - |**F**(calc)| as Fourier coefficients, written as,

$$\rho(xyz) = \frac{1}{V}\Sigma[2\,|\mathbf{F}(\mathrm{obs})| - |\mathbf{F}(\mathrm{calc})|\,]\exp[-2\pi i(hx + ky + lz) + i\alpha(\mathrm{calc})],$$

where α(calc) are the phase angles calculated for the model. This map can be regarded as the sum of the electron density of the model and of a difference electron density at normal height and provides informations for the unknown structures which are not included or are wrong in the model.

The structure was built and refined by the method of simulated annealing through alternating cycles using the program O and X-PLOR, respectively. Simulated annealing is using molecular dynamics technique, in which the dynamic behavior of a system of particles is simulated. This simulation yields an ensemble of structures that is energetically allowed for given temparature and pressure. The energy of the structures distribute followed by Bolzmann's law, which states that the number of structures with a potential energy ε_{pot} is proportional to $\exp[-\varepsilon_{pot}/k_0T]$; k_0 is Boltzmann's constant and T is the absolute temperature. The potential energy depends on the relative positions of the atoms and is calculated on the basis of known potential energy functions. A molecular dynamics calculation on a molecule starts with assigning to the atoms velocities derived from a Maxwelloan distribution at an appropriate temperature. At time $t = 0$, the atoms are in a starting configuration that has a potential energy E_{pot} for the entire molecule. On each atom i at position $\mathbf{r}_i$, and mass m_i, two forces which are calculated based on the derivative of the potential energy and Newtonian mechanics will be equal,

$$-E_{\mathrm{pot}}/\ \mathbf{r}_i = m_i(d^2\mathbf{r}/\ dt^2).$$

After a short time step Δt, usually in the 10^{-15} sec range, the process is repeated with the atoms in the new positions, and this cycle is repeated until E_{pot} reaches to the minimum, usually after 10^3 - 10^4 times. Actual function to be minimized is the total energy of the system, Q, which includes a crystallographic discrepancy term E_{X} as a psudoenergy and a potential energy E_{pot} for the entire molecule calculated both as above and below,

$$Q = E_{\mathrm{X}} + E_{\mathrm{pot}},$$

where,

$$E_{\mathrm{X}} = w_{\mathrm{X}} \Sigma[\,|\mathbf{F}(\mathrm{obs})| - k|\mathbf{F}(\mathrm{calc})|\,]^2,$$

and,

$$E_{\mathrm{pot}} = E_{\mathrm{bond}} + E_{\mathrm{bond\ angle}} + E_{\mathrm{torsion}} + E_{\mathrm{dihedral}} + E_{\mathrm{van\ der\ Waals}} + E_{\mathrm{electrostatic}}.$$

w_{X} is a weighting factor which controls the relative contribution of the potential energy and X-ray psudoenergy and directly determined by optimizing the free R-factor (Brünger, 1996). E_{pot} includes the potential energies of bond stretching, E_{bond}, bond angle bending, $E_{\mathrm{bond\ angle}}$, torsion potentials, E_{torsion}, van der Waals interactions, $E_{\mathrm{van\ der\ Waals}}$, and electrostatic potentials, $E_{\mathrm{electrostatic}}$.

Three regions were poorly defined in the resulting map. The first is at the loop and β-strand residues, Asp28-Gly50, which contain the switch I region connected to strand B2, and the second is at the residues of the switch II region. All residues in these regions were rebuilt on their omit maps. Omit map is 2Fo-Fc map calculated with a model which is excluded doubtful regions and introduced slight random shifts to reduce model bias. Structures of these parts were found to have large displacements from those of H-Ras (see text). The last is at the inserted residues, Glu125-Glu137, which is specific for members of the Rho-family. After several cycles of refinements incorporating solvent water molecules located at regions other than the inserted residues, we defined the residues forming a short 3_{10}-helix connected to an α-helix. The GTPγS molecule and Mg^{2+} ion were identified unequivocally by their appearance in 2Fo-Fc maps. The γ-sulfur atom of GTPγS was also identified by its appearance in Fo-Fc maps and its standard sulfur-phosphorus bond distance (1.9 Å), which is longer than the nonbridging oxygen-phosphorus bond (1.5 Å). Fo-Fc map is the calculated electron density using $|\mathbf{F}(obs)| - |\mathbf{F}(calc)|$ as Fourier coefficients like 2Fo-Fc map. This map shows the electron density of a difference electron density at half height and provides informations for the unknown structures which are not included or are wrong in the model. Three N-terminal residues have uninterpretable densities implying complex disorder.

The structure consists of one RhoA^{V14} molecule of 178 residues, one GTPγS, one Mg^{2+} ion, and 38 water molecules. The side chains of Arg5, Glu54, Arg68, and His126 are poorly defined in the current structure. There are no residues in disallowed regions as defined in PROCHECK (Laskowski *et al.*, 1993) (Fig. 4). A summary of the refinement statistics is given in Table 4. The structure was inspected and illustrated using the program QUANTA (Molecular Simulations Inc), MOLSCRIPT (Kraulis, 1991) rendered with RASTER3D (Merritt and Bacon, 1997) and GRASP (Nicholls *et al.*, 1991).

The atomic coordinates and structure factors (code 1A2B) have been submitted to the Protein Data Bank, Brookhaven National Laboratory, Upton, NY (Ihara *et al.*, 1998).

Table 1.

Crystal data of RhoA^{V14}-GTPγS

Crystal system	Orthorhombic
Space group	$P2_12_12$
Unit cell dimensions	a = 62.02 Å, b = 74.78 Å, c = 50.52 Å
	$\alpha = \beta = \gamma = 90$ °
Unit cell volume	2.34 x 10^5 Å^3 *
Z	4
V_m	2.77 Å^3/Da
V_{solv}	56 %

* Molecular weight of RhoA^{V14} is 20,547 Da, 563 Da for GTPγS, and 24 Da for Mg^{2+} ion.

Table 2.
Intensity data processing of RhoA^{V14}-GTPγS crystals

Resolution	2.4 Å
R_{merge} *	8.75 % (26.7 %)†
Number of measurements	61,579
Number of independent reflections	8,683
Completeness	89.3 % (74.8 %)†
Mean $<I/\sigma(I)>$	7.91 (2.04)†

* $R_{merge} = 100 \times |I(\boldsymbol{h}) - <I(\boldsymbol{h})>| / I(\boldsymbol{h})$, where $<I(\boldsymbol{h})>$ is the mean intensity for reflection $\boldsymbol{h}$.

† Brackets are quantities calculated in the highest resolution bin at 2.5-2.4 Å.

Table 3.
Solutions of rotation function and translation function *

	α	β	γ	X	Y	Z	C	R
P222	126.54	83.97	160.34	0.4270	0.4686	0.1824	32.3	52.0
	126.54	83.97	160.34	0.9963	0.0129	0.0529	32.3	52.1
	126.54	83.97	160.34	0.0591	0.4308	0.3744	31.9	51.9
	107.98	77.61	350.17	0.1120	0.0188	0.3812	31.6	51.4
	107.98	77.61	350.17	0.1115	0.0204	0.1102	31.4	51.5
	126.54	83.97	160.34	0.4204	0.4305	0.3854	31.3	52.0
	107.98	77.61	350.17	0.4322	0.4897	0.0917	31.2	51.8
	53.66	90.00	339.64	0.4739	0.3920	0.4861	31.1	51.6
	126.54	83.97	160.34	0.9994	0.4788	0.0621	31.0	52.2
	126.54	83.97	160.34	0.9963	0.0529	0.0635	31.0	51.7
$P222_1$								
	172.44	53.74	254.88	0.1833	0.0067	0.0214	33.3	50.7
	172.44	53.74	254.88	0.1839	0.3304	0.0209	33.1	51.0
	172.44	53.74	254.88	0.4306	0.3659	0.2284	32.7	51.3
	172.44	53.74	254.88	0.4314	0.3622	0.2966	31.9	51.4
	172.44	53.74	254.88	0.4316	0.3634	0.4424	31.8	51.7
	172.44	53.74	254.88	0.0486	0.4250	0.2849	31.6	52.3
	172.44	53.74	254.88	0.4314	0.3697	0.0136	30.8	51.5
	172.44	53.74	254.88	0.4673	0.3417	0.2254	30.5	52.3
	172.44	53.74	254.88	0.4292	0.3198	0.2291	30.5	52.5
	166.92	72.47	84.22	0.4794	0.0566	0.1380	30.0	52.5
$P2_12_12$								
	126.54	83.97	160.34	0.2291	0.3168	0.3688	35.2	50.1
	53.67	90.00	339.64	0.2728	0.3164	0.1317	32.7	51.1
	126.54	83.97	160.34	0.0203	0.0702	0.3713	32.1	51.9
	126.54	83.97	160.34	0.0247	0.0333	0.3637	31.6	52.1
	126.54	83.97	160.34	0.2279	0.3183	0.3126	31.2	51.7
	126.54	83.97	160.34	0.4616	0.4508	0.0150	31.2	51.8
	126.54	83.97	160.34	0.0211	0.0712	0.0105	30.9	52.1
	126.54	83.97	160.34	0.2304	0.0678	0.3704	30.7	51.6
	11.72	68.79	139.92	0.1468	0.0468	0.4078	30.7	51.8
	53.67	90.00	339.64	0.2699	0.0627	0.1422	30.6	52.0
$P2_12_12_1$								
	126.53	83.94	160.35	0.4813	0.2995	0.1202	31.3	51.3
	126.53	83.94	160.35	0.4793	0.1741	0.1191	31.2	51.1
	126.53	83.94	160.35	0.2690	0.1680	0.1182	31.0	51.4
	126.53	83.94	160.35	0.4791	0.1837	0.4861	30.7	51.4
	32.14	90.00	27.21	0.0792	0.2588	0.3072	30.5	51.6
	126.53	83.94	160.35	0.0153	0.2403	0.1820	30.4	51.8
	107.96	77.46	350.20	0.2012	0.0586	0.0759	30.3	51.6
	126.53	83.94	160.35	0.2704	0.3808	0.1211	30.3	51.7
	53.66	90.00	339.58	0.0212	0.1017	0.3831	30.2	51.9
	53.66	90.00	339.58	0.0217	0.0707	0.3816	30.1	52.6

---

* This table includes the top ten ranking of the molecular replacement solutions sorting by the correlation coefficient *C*, and *R*-factor (see text) for the respective space groups. (α, β, γ) are the Eulerian angles and (*X*, *Y*, *Z*) are the fractions of the unit cell axes. Space group $P2_12_12$ gave both the highest *C* and the lowest *R*. These calculations used the reflections between 3-6 Å and the radius of integration is 20 Å.

Table 4.
Refinement statistics

R_{cryst} *	19.5 %
R_{free} †	26.8 %
R.m.s. bond lengths	0.010 Å
R.m.s. bond angles	1.314 °
R.m.s. dihedral angles	22.368 °
R.m.s. $\Delta\omega$ ¶	1.099 °

---

* $R_{\text{cryst}} = 100 \times |F_o(\boldsymbol{h}) - F_c(\boldsymbol{h})| / F_o(\boldsymbol{h})$, where $F_o(\boldsymbol{h})$ and $F_c(\boldsymbol{h})$ are observed and calculated reflections.

† R_{free} is R_{cryst} which was calculated using 10 % of the data, chosen randomly and omitted from the subsequent molecular replacement and structure refinement.

¶ $\Delta\omega$ is the derivation of the peptide torsion angle from 180 °.

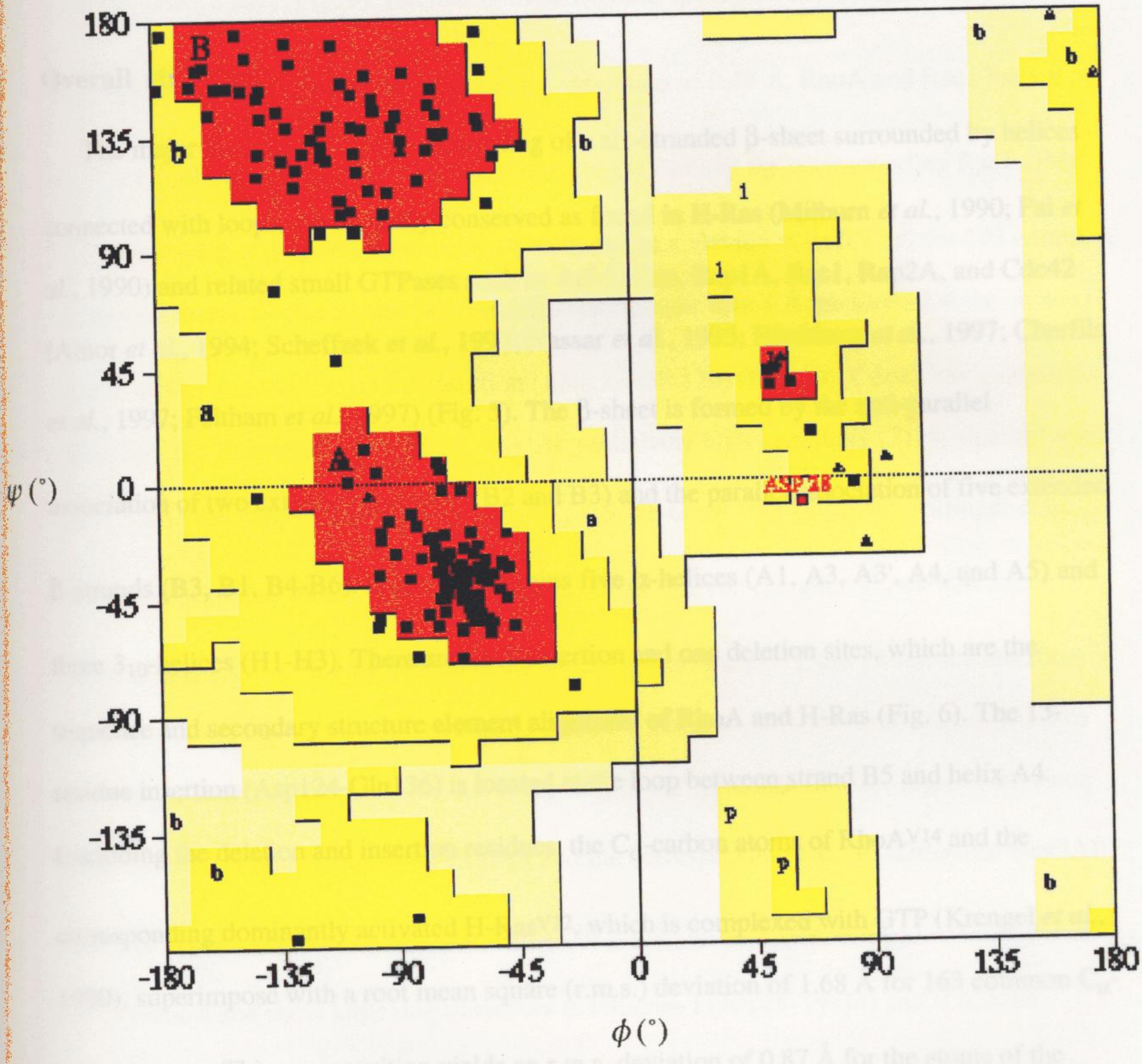

Fig. 4. Ramachandran plot of RhoA^{V14}-GTPγS.
Main chain dihedral angles were analyzed with program PROCHECK (Laskowski *et al.*, 1993). The horizontal axis indicates ϕ angle around N-C$_\alpha$ bond and the vertical axis indicates ψ angle around C$_\alpha$-C bond. Most favoured, additional allowed, generously allowed, and disallowed regions are shaded in red, yellow, light yellow, and white, respectively. Glycine residues are shown as triangles and non-glycene residues are indicated by squares. The labels A and a indicate the regions for α-helix, B and b for β-strand, and L and l for α_L-helix. There are 88.5 % of non-glycine and non proline residues in most favoured regions and no residues in disallowed regions. Asp28 in l region is indicated in red.

Results

Overall structure

The major features of the fold, consisting of a six-stranded β-sheet surrounded by helices connected with loops, are basically conserved as found in H-Ras (Milburn *et al.*, 1990; Pai *et al.*, 1990) and related small GTPases such as Arf-1, Ran, Rap1A, Rac1, Rap2A, and Cdc42 (Amor *et al.*, 1994; Scheffzek *et al.*, 1995; Nassar *et al.*, 1995; Hirshberg *et al.*, 1997; Cherfils *et al.*, 1997; Feltham *et al.*, 1997) (Fig. 5). The β-sheet is formed by the anti-parallel association of two extended β-strands (B2 and B3) and the parallel association of five extended β-strands (B3, B1, B4-B6). RhoA^{V14} contains five α-helices (A1, A3, A3', A4, and A5) and three 3_{10}-helices (H1-H3). There are three insertion and one deletion sites, which are the sequence and secondary structure element alignment of RhoA and H-Ras (Fig. 6). The 13-residue insertion (Asp124-Gln136) is located at the loop between strand B5 and helix A4. Excluding the deletion and insertion residues, the C_α-carbon atoms of RhoA^{V14} and the corresponding dominantly activated H-Ras^{V12}, which is complexed with GTP (Krengel *et al.*, 1990), superimpose with a root mean square (r.m.s.) deviation of 1.68 Å for 163 common C_α-carbon atoms. This superposition yields an r.m.s. deviation of 0.87 Å for the atoms of the guanine nucleotide. Segments that involve major differences are located at the switch I and II regions and part of the antiparallel β-sheet, consisting of the C-terminal half of strand B2 and the N-terminal half of strand B3, in addition to the insertion and deletion sites described above (Fig. 7). Recently, Wei *et al.* have reported the crystal structure of RhoA bound to GDP (Wei *et al.*, 1997). Compared with this to RhoA-GDP structure, the significant conformational changes were found to be localized in the switch I (Asp28-Ala44) and II (Gly62-Arg68) regions (Fig. 8), as described for H-Ras (Milburn *et al.*, 1990; Tong *et al.*, 1991), while, the lengths and positions of these regions are differ from the Ras family GTPases (Milburn *et al.*, 1990; Cherfils *et al.*, 1997) (Fig. 9). Excluding these regions, the C_α-carbon atoms of RhoA^{V14}-GTP γS and RhoA-GDP superimpose with a r.m.s. deviation of 0.48 Å. RhoA and Rac1 have a sequence homology with 56 % identity. RhoA^{V14}-GTPγS and the corresponding Rac1-GMP-PNP (Hirshberg *et al.*, 1997) superimpose with an r.m.s. deviation of 0.77 Å for 173 common C_α-carbon atoms. Segments that involve differences larger than 1 Å are located at the switch I (Val33-Ile46) and the 13-residue insertion (Asn123-Gln136) (Fig. 10). Cdc42 has a sequence homology (52 % identity) with RhoA, but has a relatively high homology (71 % identity) with Rac1, RhoA^{V14}-GTPγS and the corresponding Cdc42-GMP-PNP-rhoGAP (Rittinger *et al.*, 1997a) superimpose with a r.m.s. deviation of 0.90 Å for 165 common C_α-carbon atoms. Major differences are mainly located at the switch I (Gln29-Lys51), the 13-residue insertion (Ala132-Glu142) and the region of His105-Asn109. These regions are well corresponded to those in the superposition with Rac1, but the lengths and positions of these regions are some what different (Fig. 11). RhoA^{V14}-GTPγS and the corresponding RhoA-GDP-AlF_4^--rhoGAP (Rittinger *et al.*, 1997b) superimpose with a r.m.s. deviation of 0.52 Å for 173 common C_α-carbon atoms and show large displacements at switches I (Asp28-Tyr34) and II (Glu64, Asp65) (Fig. 12). The nonhydrolyzable nucleotide GTPγS binds to the protein by the similar way to H-Ras-GMP-PNP (Pai *et al.*, 1990) (Fig. 13), and a Mg^{2+} ion shows a typical octahedral coordination sphere (Fig. 14).

Insertion regions

The N-terminal segment (Glu125-Lys133) of the 13-residue insertion forms an α-helix designated as A3', which is followed by an extended loop. A short 3_{10}-helix, designated as H3 (Fig. 5), is induced at the segment flanking the N-terminus of this insertion, with large displacements of Arg122 and Asn123 from those of H-Ras^{V12} (3.0 Å and 6.1 Å, respectively). Compared with RhoA-GDP, however, no significant conformational change exists in the 13-residue insertion and its N-terminal flanking regions. This folding seems to be basically similar to that of Rac1 complexed with GMP-PNP (Hirshberg *et al.*, 1997) but shows many differences in details. It is notable that the sequences of this region of members in the Rho subfamily is rather different from those of the Rac subfamily. Among the key residues in stabilization of helices H3 and A3' (Fig. 15), Arg122 and Asp124 are conserved in the Rho family but Arg128, Glu137, and Lys140 are variant in the Rac subfamily. No water molecule is found to be involved in the structural stabilization of the RhoA insertion region, though Rac1 forms a water-mediated hydrogen bond between the main chains. The conserved residues Leu131 and Pro138 of helix A3' form a hydrophobic patch with Thr127 and Pro89, which are also conserved or conservatively replaced in the Rho family. Rac1 adds Ile126 (Arg128 of RhoA) to the hydrophobic patch.

The outer surface of helix A3' is covered with charged residues whose side chains form hydrogen bonds and/or ion pairs, Glu125-Arg129 and Glu130-Lys133 pairs. These residues are conserved or conservatively substituted in Rho subfamily, but are replaced by other amino acid residues in the Rac subfamily. It is interesting that, in the Rac subfamily, Glu125 and Arg129 are substituted by lysine and glutamic acid, respectively, and Glu130 and Lys133 are substituted by lysine/arginine and glutamic acid, respectively. Therefore, these pairs of acidic and basic residues of Rac1 could form hydrogen bonds or ion pairs as observed in the current structure, though most of the exposed side chains of the residues of Rac1 corresponding to the residues 125-135 of RhoA are highly mobile.

Compared with H-Ras, helix A3 has a one-residue insertion at the center and two Pro residues (Pro96 and Pro101), which cause a disruption of the normal hydrogen-bonding pattern of an α-helix, whereas H-Ras has no Pro residue on this helix. These differences induce a relatively large discrepancy (2.05 Å at Pro96) of helix A3 from that of H-Ras^{V12} (Fig. 7). Both Pro96 and Pro101 face the solvent region so as to induce pronounced kinks that serve to maximize the contacts with strands B1 and B4.

Phosphate-binding loop

The G14V mutation of RhoA and the G12V mutation of H-Ras exhibit less than one-tenth the GTPase activity of the wild-type GTPases. Crystal structures of H-Ras^{V12} complexed with GDP (Milburn *et al.*, 1990; Tong *et al.*, 1991) and GTP (Krengel *et al.*, 1990) show that the mutation causes no significant conformation change at the phosphate-binding region, though there are large differences in mobility and conformation predominantly localized in the switch II region (see below). Similar results were obtained in RhoA. The r.m.s. deviation of the ^{12}GXG(V)XXGKT/S^{19} motifs between RhoA^{V14}-GTPγS and RhoA-GDP is small (0.31 Å) and that between RhoAV14-GTPγS and H-Ras^{V12}-GTP is relatively small (0.84 Å). However, the bulky side chain of Val14 contacts with Gly62 and Gln63, and these contacts cause a displacement (0.71 Å) of the C_α-carbon atom of Val14 from the corresponding atom of the wild-type RhoA (Fig. 16).

Switch I

The switch I region in RhoA^{V14}-GTPγS is well ordered in the crystal structure as well as that of RhoA-GDP. In contrast, in Rac1-GMP-PMP, residues 32-36 of switch I (34-38 in RhoA) are disordered. Dramatic changes in the conformations of switch I and its C-terminal flanking regions, as compared with RhoA-GDP, occurs with the largest displacements (5.4 Å and 6.4 Å) at Pro36 and Phe39, respectively (Fig. 16). Similar conformational changes whether bound to GTP or GDP were reported for H-Ras (Milburn *et al.*, 1990; Schlichting *et al.*, 1990), and the G_α subunits of the trimeric GTPases such as transducin-α (Lambright *et al.*, 1994), thereby playing a key role as a molecular switch in signal transduction. Tyr34 and Pro36 of RhoA^{V14} flip their side chains toward the nucleotide so as to shield the triphosphate group from the solvent region. The phenolic ring of Tyr34 stacks on the Pro36 and also contacts with Ala15 and Val14 to close the entrance of the phosphate-binding pocket. These conformational changes are accompanied by the flipping out of hydrophobic residues, Val33, Val35, Val38, and Phe39, toward the solvent region. It should be noted that Val38 and Phe39 form a hydrophobic patch on the molecular surface together with Tyr66 and Leu69 of switch II. These contacts play a pivotal role to induce the stable conformation of switch II (see below). Switch I of RhoA^{V14} displays a significantly different conformation from that of H-Ras^{V12}-GTP. Large displacements of the residues of switch I begin from Asp28 and end at Pro36 with the largest displacement (4.1 Å) at Glu32 (Fig. 17). These displacements, which result in differences in recognition of the ribose of the guanine nucleotide, seem to be caused by Pro31, which restricts the main chain torsion angles. Since Pro31 is well conserved in the Rho-family but is replaced by other residues in Ras (Val), Rab (Val), and Ran (Asp), the displacements could be a common structural feature of members of the Rho family. While large displacements were observed in switch I as described, no significant difference in the position and orientation of Thr37, which coordinates to the Mg^{2+} ion, is seen between RhoA^{V14} and H-Ras^{V12}.

Strand B2 and B3

The switch I loop is connected to the anti-parallel β-sheet of strands B2 and B3, which is followed by switch II. This two-stranded sheet is located at the edge of the six-stranded β-sheet and is sitting on helices A1 and A5 to form a hydrophobic core. Compared with H-Ras^{V12}-GTP, a large displacement of these strands expands between a stretch from Ala44 to Val53, which moves toward helices A1 and A5, with the largest shift being 2.9 Å at Asp45. It is notable that the sequence of this region is highly conserved in the Rho subfamily. This displacement seems to be caused mainly by differences in hydrophobic interactions between these strands and helices A1 and A5. Strands B2 and B3 are connected by a reverse turn of type II formed by ^{48}VDGK^{51}. H-Ras^{V12} and H-Ras also have a type II reverse turn at this position with the corresponding segment, ^{46}IDGE^{49}. Since the third residue of this type of reverse turn should have a Gly residue to avoid the steric clash with the main-chain carboxyl group of the second residue, mutations of this residue to any other residue destroy the reverse turn, which results in large conformational changes of the strands or displacement of the β-sheet. This may possibly explain why mutations of Gly48 in H-Ras inhibits effector function (Der *et al.*, 1986) even though this residue is distal from the effector-binding site encompassing switch I and the N-terminal half of strand B2, as observed in the crystal of Rap1A-Raf1 complexes (Nassar *et al.*, 1995).

Switch II

The segment between strands B3 and B4 contains the switch II region that has a key residue Gln63 (Gln61 of H-Ras) of GTPase activities. Mutation of Gln61 of H-Ras to almost any other amino acid blocks intrinsic and GAP-stimulated GTPase activity (Marshall, 1993). In the crystal structures of cellular H-Ras complexed with either GDP (Milburn *et al.*, 1990), GMP-PCP (Tong *et al.*, 1991), or GMP-PNP (Pai *et al.*, 1990), the highly conserved ^{57}DTAGQE^{62} motif of switch II exhibits flexibility to adapt to alternative conformations although this motif of oncogenic H-Ras^{V12} complexed with GTP has only one major conformation (Krengel *et al.*, 1990). In RhoA-GDP, residues 63-65 are also disordered. The electron density of this region of RhoA^{V14} is well defined and has a single conformation at the present resolution. RhoA^{V14} has two 3_{10}-helices, H1 (^{64}EDY^{66}) and H2 (^{70}RPL^{72}), which are separated by a short loop of three residues (^{67}DRL^{69}). The sequence of this region is well conserved in the Rho family but is different from those regions in the Ras family (Fig. 6). A similar conformation is also seen in the crystal structure of Rac1-GMP-PNP. In contrast, H-Ras^{V12} has a 3_{10}-helix at the position corresponding to the short loop of RhoA^{V14} with an α-helix of five residues corresponding to residues 71-75 of RhoA^{V14}. These differences induce a large displacement of Glu64 (3.8 Å), together with reorientations of the side chains of Gln63, Glu64 and Asp65 from the corresponding residues of H-Ras^{V12} (Fig. 7). Lys98 and Glu102, both of which are located at helix A3, play crucial roles in the conformation of the segment by forming multiple hydrogen bonds to switch II (Fig. 18). These two residues are conserved in members of the Rho family but are replaced in H-Ras. Moreover, the segment from helices H1 to H2 makes hydrophobic contacts strands B2 and B3. In this hydrophobic core, H-Ras^{V12} has an additional residue Tyr71, which is replaced by a small residue (Ser73) in RhoA. This difference causes a movement of the helix H2 toward strand B2. These differences seem to be one of the main reasons why the conformations of the segment are so different between RhoA^{V14} and H-Ras^{V12}.

Magnesium ion binding

The strong GTP/GDP-binding and the GTPase activity of small GTPases have been shown to be absolutely dependent on the presence of divalent ions. The Mg^{2+} ion of the present structure is located at a position similar to those in H-Ras^{V12}-GTP and in H-Ras-GMP-PNP, as well as that in RhoA-GDP. The displacement of the ion from the corresponding position in the GDP-bound form is 1.04 Å. The Mg^{2+} ion plays a key role in bridging together the functional regions of the phosphate-binding, switch I and II, as observed in H-Ras. Actually, the stereochemistry of Mg^{2+} coordination is identical to that in H-Ras-GMP-PNP. In contrast, the stereochemistry of Mg^{2+} coordination in RhoA-GDP is different from the current form but also is different from that in H-Ras-GDP.

Guanosine nucleotide binding

The glycosyl conformation of GTPγS is *anti* with C2'-*endo* sugar pucker. The guanosine base is trapped in a hydrophobic pocket, in a manner similar to H-Ras^{V12}-GTP, to be recognized by several interactions with the conserved residues of the ^{116}GXKXDL^{121} and ^{160}SAK^{162} motifs (Fig. 17). A major difference in base recognition is the water-mediated hydrogen bonds to the N7 and O6 atoms of the guanine base. The water molecule (Wat-1) is completely buried inside the hydrophobic binding pocket with a hydrogen bond to Gly17. The space for the accommodation of this water molecule is mainly produced by a rearrangement of the side-chain packing of the pocket, involving Leu21, Asn117, and Cys159 (Fig. 19). In H-Ras, Cys159 of RhoA is replaced by a Thr residue. In addition to the base recognition, the 2'-hydroxyl group of the ribose also has a water-mediated hydrogen bond to switch I (Wat-2), although in H-Ras^{V12}-GTP the hydroxyl group of the ribose forms direct hydrogen bonds with the main-chains corresponding to Pro31 and Glu32 of RhoA. As mentioned above, these differences in the recognition of the ribose are caused by the large displacements of switch I. Similar water-mediated hydrogen bonds in base and sugar recognition have also been found in RhoA-GDP and in Rac1-GMP-PNP.

Triphosphate binding

GTP and GDP bind to small GTPases with dissociation constants on the order of nanomolar. This strong binding affinity is well demonstrated in the current structure. The triphosphate moiety of GTPγS has 21 direct and 9 water-mediated hydrogen bonds to the protein, together with 2 magnesium coordinations. These involve six residues of the phosphate-binding loop, four residues of switch I, three residues of switch II, and four residues of base-recognition motifs. It is notable that most of these residues of the phosphate-binding loop interact with the triphosphate through their main-chains, especially the amino groups. This is the reason why the amino acid sequence of the ^{12}GXGXXGKT/S^{19} motif contains many variant residues. The residues whose side chains participate in the interactions with the triphosphate are invariant Lys18, Tyr34, and Asp59. The conformation of the triphosphate exhibits similarity to that of GDP bound to RhoA, with relatively small displacements of the α- and β-phosphates from those of GDP, 0.75 Å and 0.67 Å, respectively. Two oxygen atoms of the γ-phosphate make contact with the protein by several hydrogen bonds, together with the coordination to the Mg^{2+} ion buried inside the pocket formed by switches I and II and the phosphate-binding loops. These heavy interactions allow the γ-phosphate to orient the γ-sulfur atom toward Val14, Tyr34, and Pro36. Similar configurations of the γ-thiophosphate were also observed in the crystal structures of transducin-α (Noel *et al.*, 1993) and $G_{i\alpha 1}$ (Coleman *et al.*, 1994) complexed with GTPγS. In all these crystals complexed with GTPγS, the γ-sulfur atom is the closest atom to the side-chain amide group of Gln63 (Gln200 of transducin-α and Gln204 of $G_{i\alpha 1}$) among the γ-thiophosphate atoms.

Putative nucleophilic water molecule

We identified one water molecule (Wat-3) that is close enough to the γ-phosphate to perform an in-line nucleophilic attack. The water molecule is located at a position 10 ° off from this line at a distance of 3.6 Å from the phosphorus atom and forms a hydrogen bond (3.3 Å) to the γ-sulfur atom, although the distance to the γ-oxygen atoms of the phosphate group is too long to form a hydrogen bond (3.6 Å for both). Similar water molecules have been located in analogous positions close to the γ-phosphate in the crystal structures of transducin-α and $G_{i\alpha 1}$ complexed with GTPγS, as well as of H-Ras, Rac1, and EF-Tu (Berchtold *et al.*, 1993) complexed with GMP-PNP, although no water molecule corresponding to Wat-3 has been found in RhoA-GDP. Gln63 positions the side-chain oxygen atom at a distance of 3.8 Å from the hydrolytic water and the side-chain nitrogen atom at a distance of 3.8 Å from the side-chain carboxyl group of Asp65.

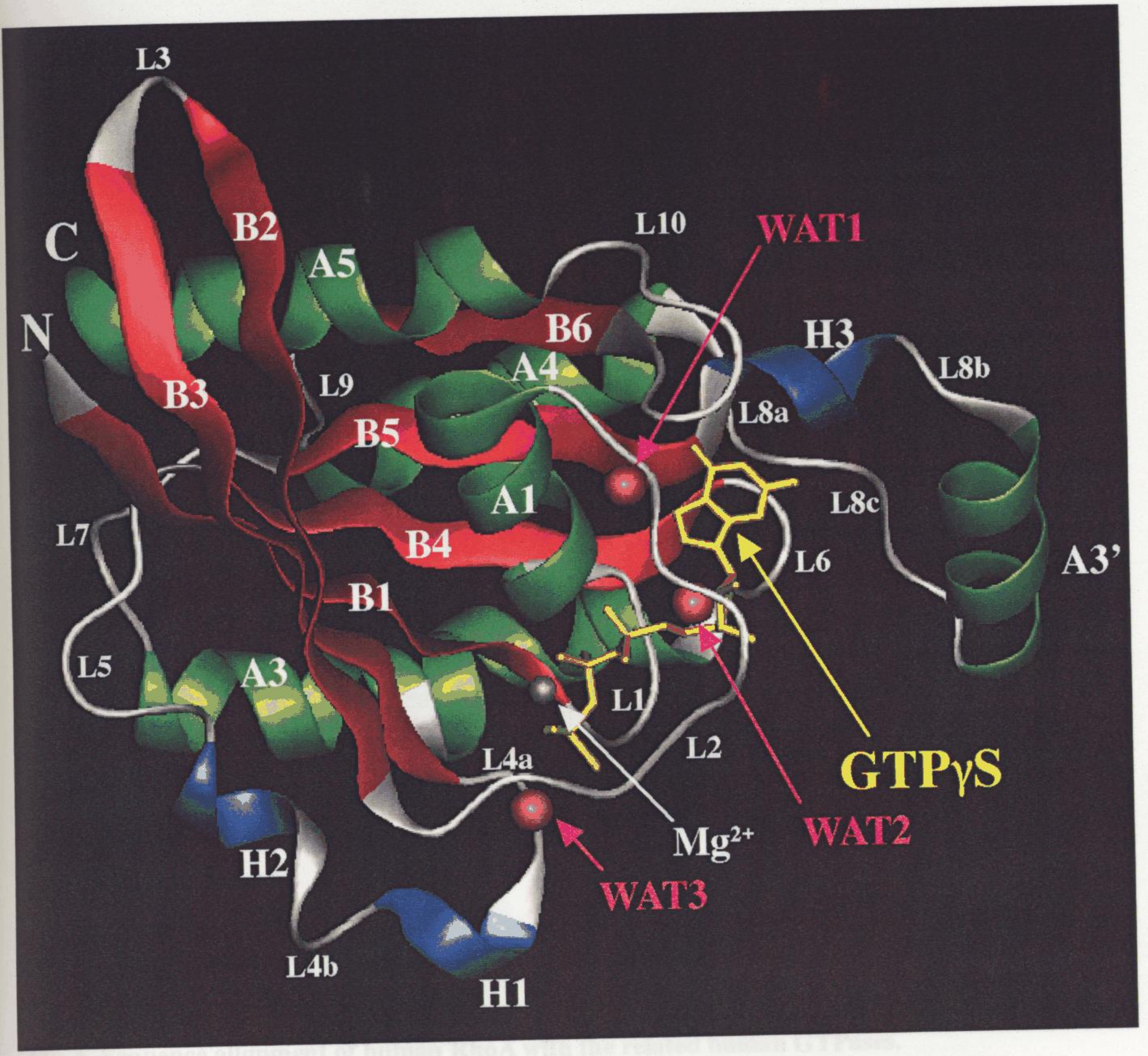
L3
C
B2
A5
L10
WAT1
N
B6
H3
A4
L8b
B3
L9
L8a
B5
A1
L8c
L7
B4
L6
A3'
B1
L5
A3
L1
L2
GTPγS
L4a
Mg2+
WAT2
H2
WAT3
L4b
H1

Fig. 5. Structure of RhoA^{V14}-GTPγS.

Ribbon representation of RhoA^{V14} complexed with GTPγS (yellow) and Mg^{2+} (a gray ball) with β-strands (red), α-helices (green), and 3_{10}-helices (blue) is shown. Three water molecules (pink balls) are also illustrated. One water molecule (Wat1) participates in the guanine-base recognition of GTPγS, the second (Wat2) participates in the binding of the ribose, and the last (Wat3) is a putative nucleolytic water molecule. The secondary structure elements, Mg^{2+} ion, water, and GTP molecules are labeled as well as the N- and C-termini.

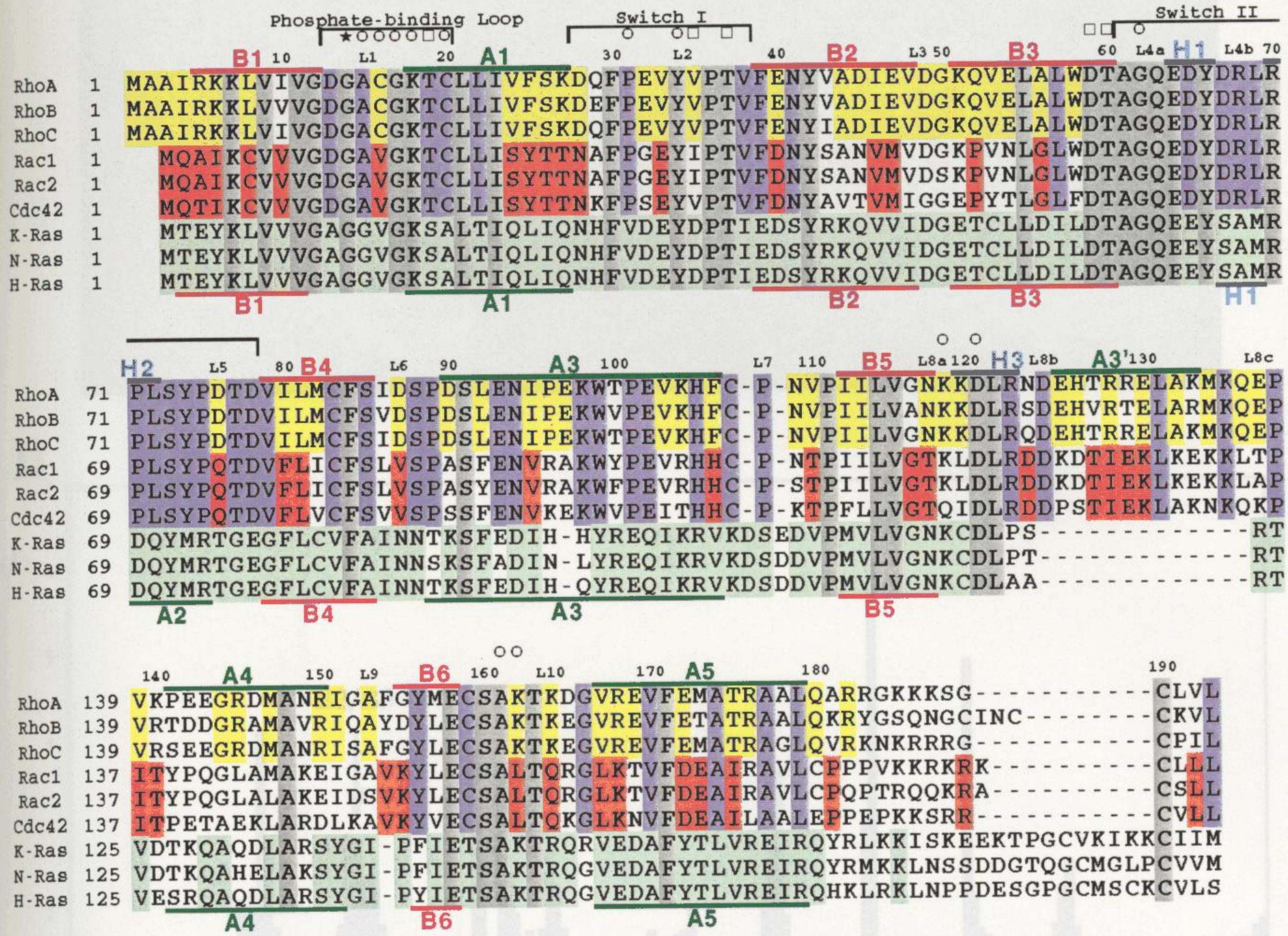

```
RhoA    1  MAAIRKKLVIVGDGACGKTCLLIVFSKDQFPEVYVPTVFENYVADIEVDGKQVELALWDTAGQEDYDRLR
RhoB    1  MAAIRKKLVVVGDGACGKTCLLIVFSKDEFPEVYVPTVFENYVADIEVDGKQVELALWDTAGQEDYDRLR
RhoC    1  MAAIRKKLVIVGDGACGKTCLLIVFSKDQFPEVYVPTVFENYIADIEVDGKQVELALWDTAGQEDYDRLR
Rac1    1    MQAIKCVVVGDGAVGKTCLLISYTTNAFPGEYIPTVFDNYSANVMVDGKPVNLGLWDTAGQEDYDRLR
Rac2    1    MQAIKCVVVGDGAVGKTCLLISYTTNAFPGEYIPTVFDNYSANVMVDSKPVNLGLWDTAGQEDYDRLR
Cdc42   1    MQTIKCVVVGDGAVGKTCLLISYTTNKFPSEYVPTVFDNYAVTVMIGGEPYTLGLFDTAGQEDYDRLR
K-Ras   1    MTEYKLVVVGAGGVGKSALTIQLIQNHFVDEYDPTIEDSYRKQVVIDGETCLLDILDTAGQEEYSAMR
N-Ras   1    MTEYKLVVVGAGGVGKSALTIQLIQNHFVDEYDPTIEDSYRKQVVIDGETCLLDILDTAGQEEYSAMR
H-Ras   1    MTEYKLVVVGAGGVGKSALTIQLIQNHFVDEYDPTIEDSYRKQVVIDGETCLLDILDTAGQEEYSAMR

RhoA   71  PLSYPDTDVILMCFSIDSPDSLENIPEKWTPEVKHFC-P-NVPIILVGNKKDLRNDEHTRRELAKMKQEP
RhoB   71  PLSYPDTDVILMCFSVDSPDSLENIPEKWVPEVKHFC-P-NVPIILVANKKDLRSDEHVRTELARMKQEP
RhoC   71  PLSYPDTDVILMCFSIDSPDSLENIPEKWTPEVKHFC-P-NVPIILVGNKKDLRQDEHTRRELAKMKQEP
Rac1   69  PLSYPQTDVFLICFSLVSPASFENVRAKWYPEVRHHC-P-NTPIILVGTKLDLRDDKDTIEKLKEKKLTP
Rac2   69  PLSYPQTDVFLICFSLVSPASYENVRAKWFPEVRHHC-P-STPIILVGTKLDLRDDKDTIEKLKEKKLAP
Cdc42  69  PLSYPQTDVFLVCFSVVSPSSFENVKEKWVPEITHHC-P-KTPFLLVGTQIDLRDDPSTIEKLAKNKQKP
K-Ras  69  DQYMRTGEGFLCVFAINNTKSFEDIH-HYREQIKRVKDSEDVPMVLVGNKCDLPS------------RT
N-Ras  69  DQYMRTGEGFLCVFAINNSKSFADIN-LYREQIKRVKDSDDVPMVLVGNKCDLPT------------RT
H-Ras  69  DQYMRTGEGFLCVFAINNTKSFEDIH-QYREQIKRVKDSDDVPMVLVGNKCDLAA------------RT

RhoA  139  VKPEEGRDMANRIGAFGYMECSAKTKDGVREVFEMATRAALQARRGKKKSG-----------CLVL
RhoB  139  VRTDDGRAMAVRIQAYDYLECSAKTKEGVREVFETATRAALQKRYGSQNGCINC--------CKVL
RhoC  139  VRSEEGRDMANRISAFGYLECSAKTKEGVREVFEMATRAGLQVRKNKRRRG-----------CPIL
Rac1  137  ITYPQGLAMAKEIGAVKYLECSALTQRGLKTVFDEAIRAVLCPPPVKKRKRK----------CLLL
Rac2  137  ITYPQGLALAKEIDSVKYLECSALTQRGLKTVFDEAIRAVLCPQPTRQQKRA----------CSLL
Cdc42 137  ITPETAEKLARDLKAVKYVECSALTQKGLKNVFDEAILAALEPPEPKKSRR-----------CVLL
K-Ras 125  VDTKQAQDLARSYGI-PFIETSAKTRQRVEDAFYTLVREIRQYRLKKISKEEKTPGCVKIKKCIIM
N-Ras 125  VDTKQAHELAKSYGI-PFIETSAKTRQGVEDAFYTLVREIRQYRMKKLNSSDDGTQGCMGLPCVVM
H-Ras 125  VESRQAQDLARSYGI-PYIETSAKTRQGVEDAFYTLVREIRQHKLRKLNPPDESGPGCMSCKCVLS
```

Fig. 6. Sequence alignment of human RhoA with the related human GTPases.

Conserved residues are highlighted in yellow for the Rho subfamily (RhoA, RhoB, and RhoC), in red for the Rac subfamily (Rac1, Rac2, and Cdc42), in blue for the Rho family, in light green for the Ras family (K-Ras, N-Ras, and H-Ras) and gray for all members. The secondary structure elements of RhoA^{V14}-GTPγS and H-Ras^{V12}-GTP complexes are indicated at the top and below the aligned sequences, respectively. The α-helices (A1-A5) are in green, the extended β (B1-B6) are in green, and the 3_{10}-helices (H1-H3) are in blue. Three functional regions of RhoA are also indicated with marks for the residues that participate in interactions with GTPγS (circles) and the Mg^{2+} ion (rectangles). The dominantly active mutation of glycine to valine is indicated by a star. The sequences are taken from SwissProt. The accession numbers are P06749 (RhoA), P01121 (RhoB), P08134 (RhoC), P15154 (Rac1), P15153 (Rac2), P25763 (Cdc42), P01116 (K-Ras), P01111 (N-Ras), and P01112 (H-Ras).

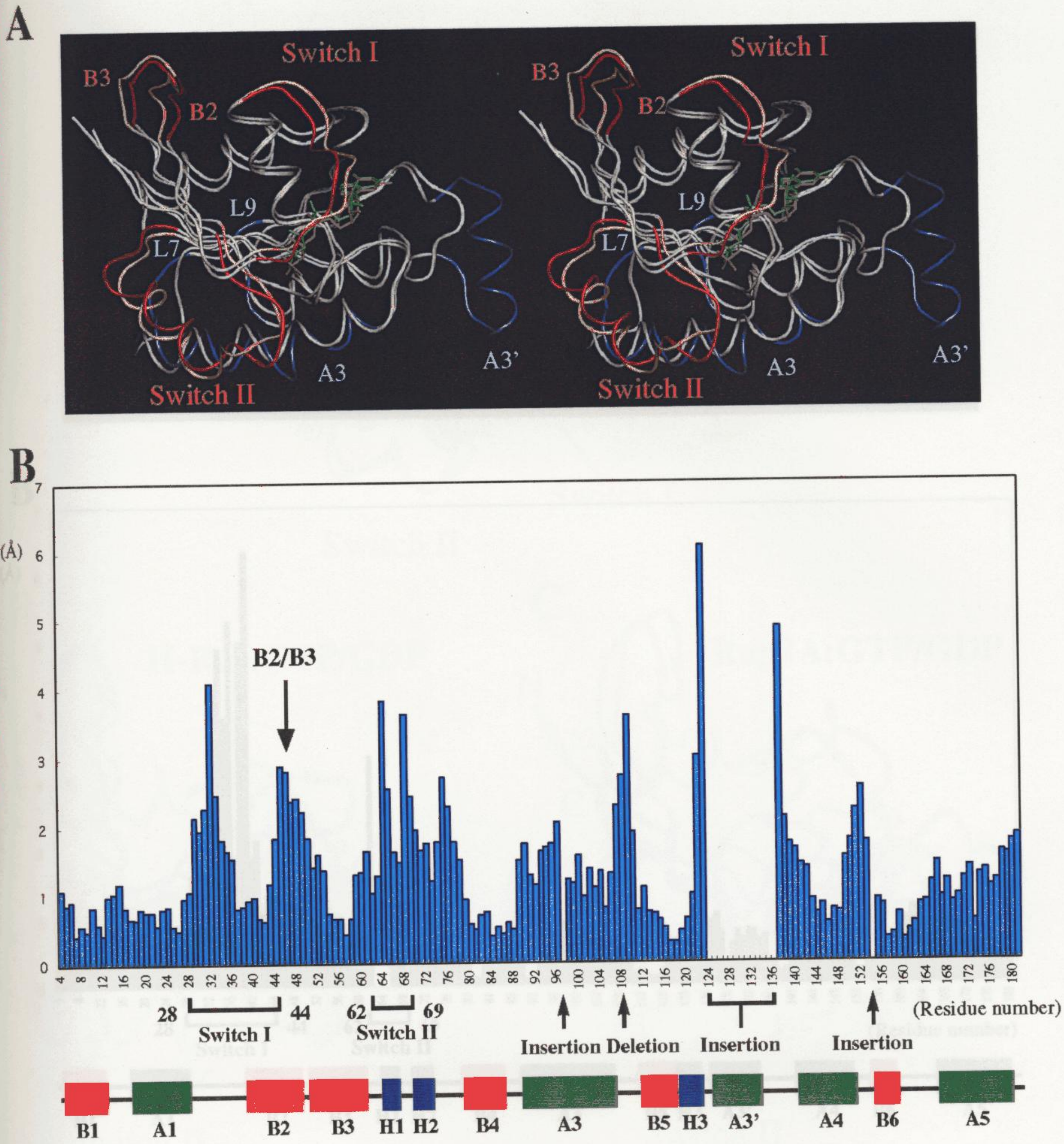

Fig. 7. Structural comparison of RhoA^{V14}-GTPγS with H-Ras^{V12}-GTP.

A, superposition of C_α-carbon atom tracings of RhoA^{V14} bound to GTPγS (magenta) and H-Ras^{V12} bound to GTP (green) (Protein Data Bank code 521P; Krengel *et al.*, 1990). Segments displaying large displacements are highlighted in red for RhoA^{V14} and yellow for H-Ras^{V12}. These include switch I (residue 27-36 for RhoA), the anti-parallel β-sheet formed by strands B2 and B3 (residues 43-53), and switch II (residues 59-78). The 13-residue insertion (residues 122-137), forming helix A3', and the segments helix A3 (residues 90-106), L7 (residues 107-110), and L9 (residues 151-154), which have insertion or deletion to produce large displacements, are in blue for RhoA^{V14}. ***B***, a histogram shows distances between the corresponding C_α-carbon atoms between RhoA^{V14}-GTPγS and H-Ras^{V12}-GTP, with the secondary structure elements of RhoA^{V14} at the bottom.

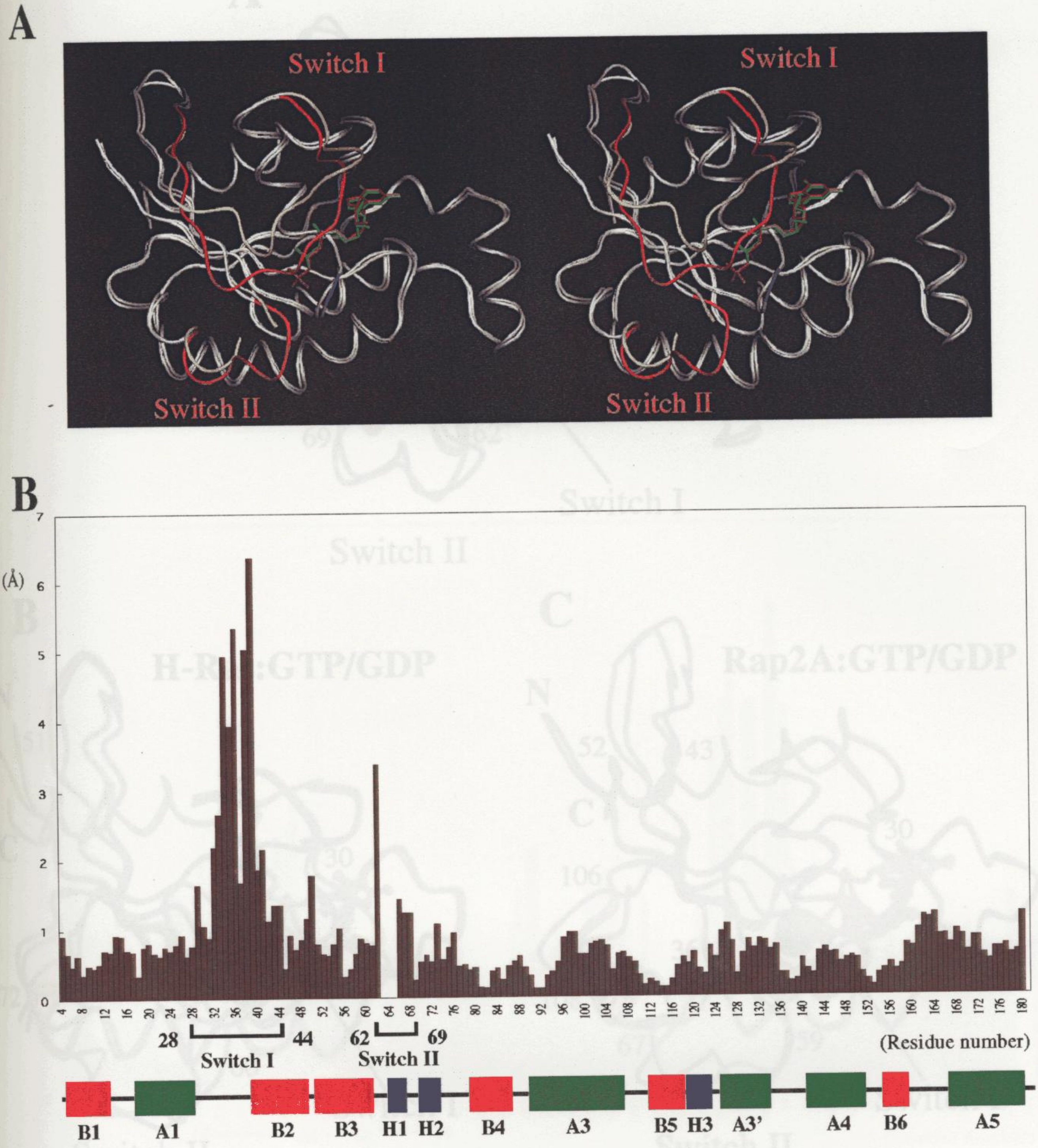

Fig. 8. Structural comparison of RhoA^{V14}-GTPγS with RhoA^{N25}-GDP.

A, superposition of C_α-carbon atom tracings of RhoA^{V14} bound to GTPγS (magenta) and RhoA^{N25} bound to GDP (green) (Protein Data Bank code 1FTN; Wei *et al.*, 1997) with segments displaying large displacements in red and yellow, respectively. These include switch I and the C-terminal flanking region (residues 28-44) and the N-terminal region of switch II (residues 62-69). Val14 of RhoA^{V14} is highlighted in blue. In RhoA^{N25}-GDP, residues 63-65 are disordered. ***B***, a histogram shows distances between the corresponding C_α-carbon atoms between RhoA^{V14}-GTPγS and RhoA^{N25}-GDP, with the secondary structure elements of RhoA^{V14} at the bottom.

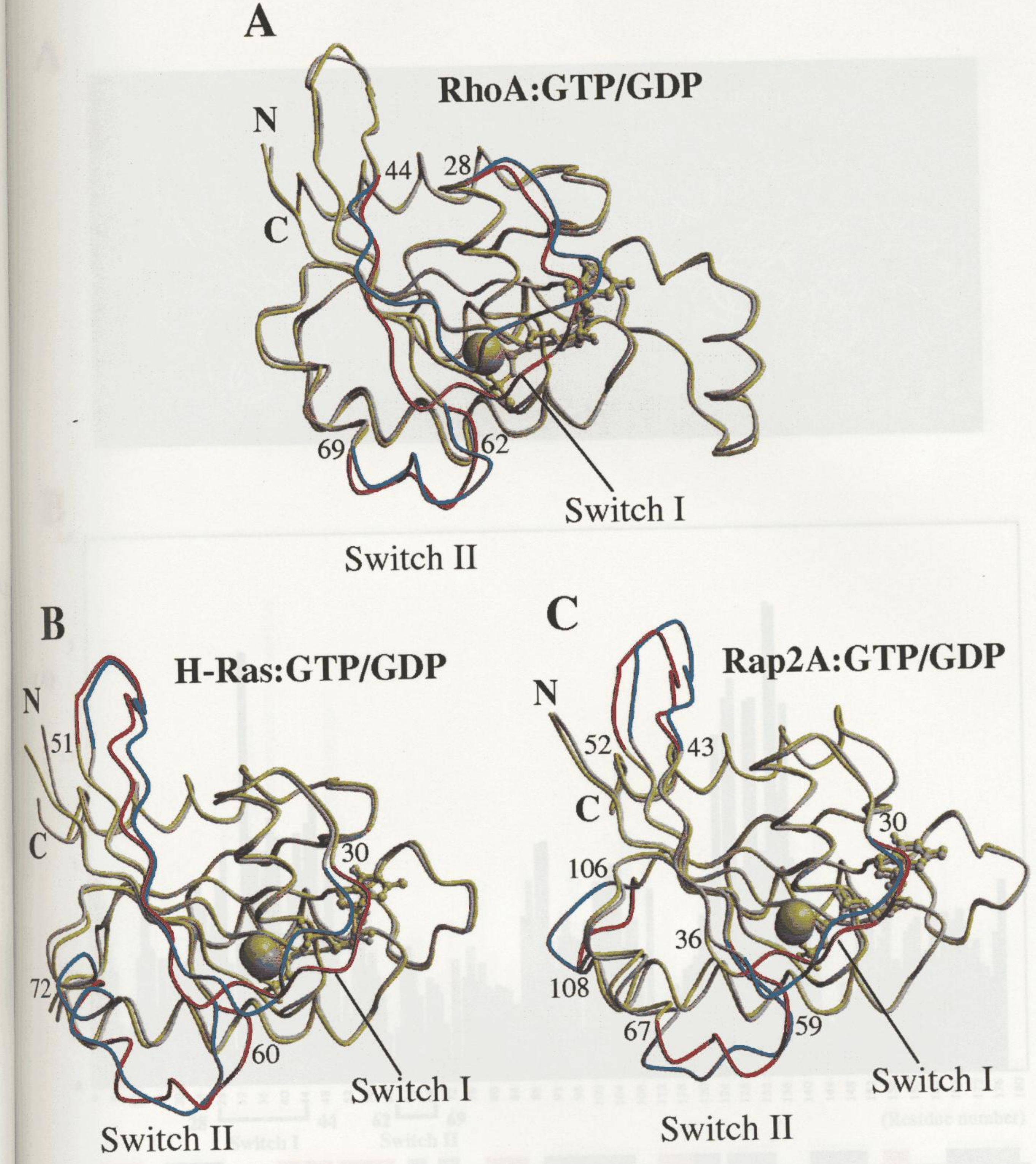
A
RhoA:GTP/GDP
N
44
28
C
69
62
Switch I
Switch II
B
H-Ras:GTP/GDP
N
51
C
30
72
60
Switch I
Switch II
C
Rap2A:GTP/GDP
N
52
43
C
30
106
36
108
67
59
Switch I
Switch II

Fig. 9. Switch regions of small GTPases.

Comparison among the known switch regions. ***A***, superposition of C_α-carbon atom tracings of RhoA^{V14}-GTPγS (yellow) and RhoA^{N25}-GDP (white). ***B***, for H-Ras-GTP (yellow) (Protein Data Bank code 5P21; Pai *et al.*, 1990) and H-Ras-GDP (white) (Protein Data Bank code 4Q21; Milburn *et al.*, 1990). ***C***, for Rap2A-GTP (yellow) (Protein Data Bank code 2RAP; Cherfils *et al.*, 1997) and Rap2A-GDP (white) (Protein Data Bank code 1KAO; Cherfils *et al.*, 1997). Segments displaying large displacements are highlighted in red for GTP forms and cyan for GDP forms with numbers of the start and the end residues. Large spheres represent Mg^{2+} ions.

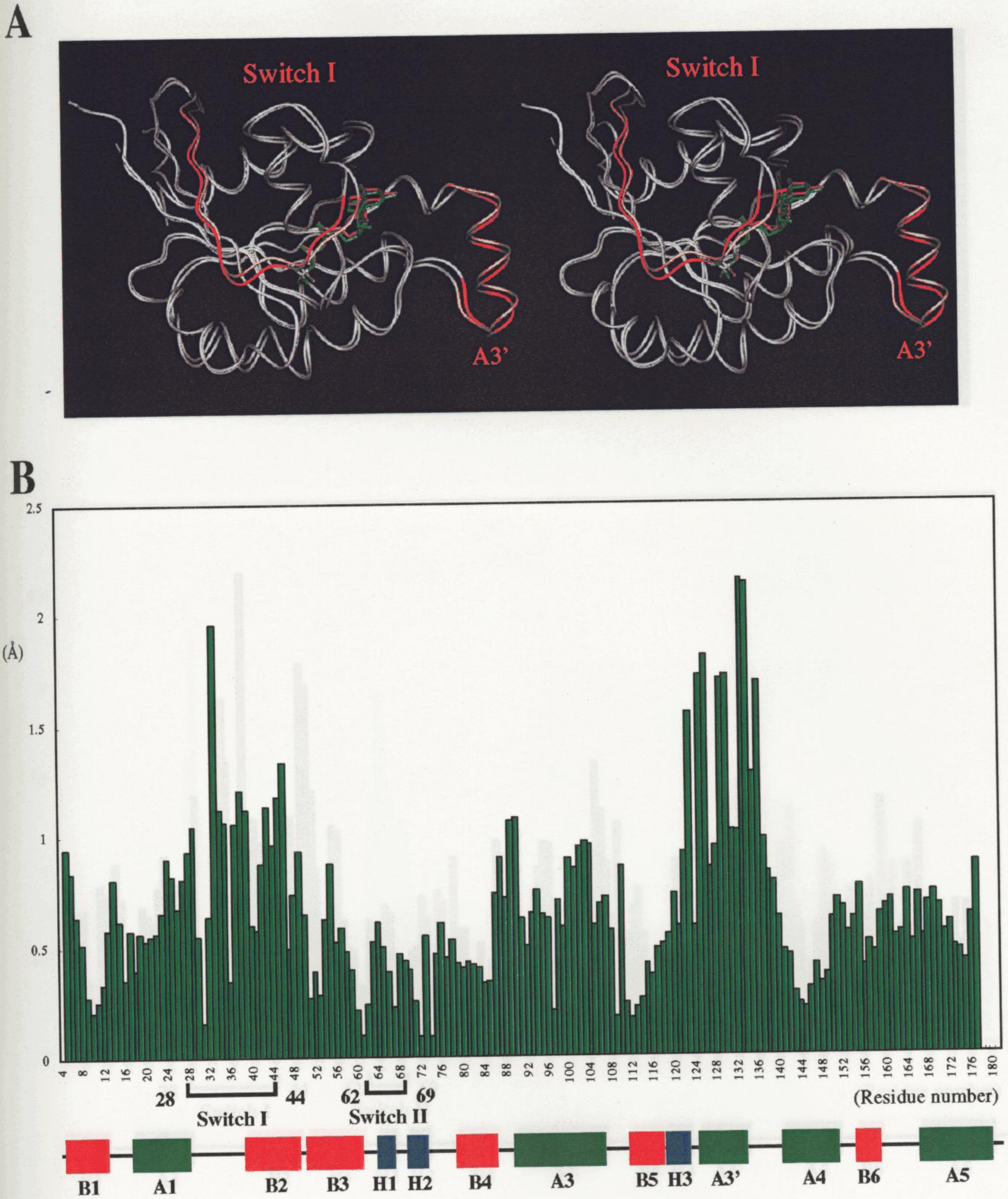

Fig. 10. Structural comparison of RhoA^{V14}-GTPγS with Rac1-GMP-PNP.
A, superposition of C_{α}-carbon atom tracings of RhoA^{V14} bound to GTPγS (magenta) and Rac1 bound to GMP-PNP (green) (Protein Data Bank code 1MH1; Hirshberg *et al.*, 1997) with segments displaying large displacements in red and yellow, respectively. These include switch I (residues 33-46 for RhoA) and the 13-residue insertion (residues 123-136), forming helix A3'. ***B***, a histogram shows distances between the corresponding C_{α}-carbon atoms between RhoA^{V14}-GTPγS and Rac1-GMP-PNP, with the secondary structure elements of RhoA^{V14} at the bottom.

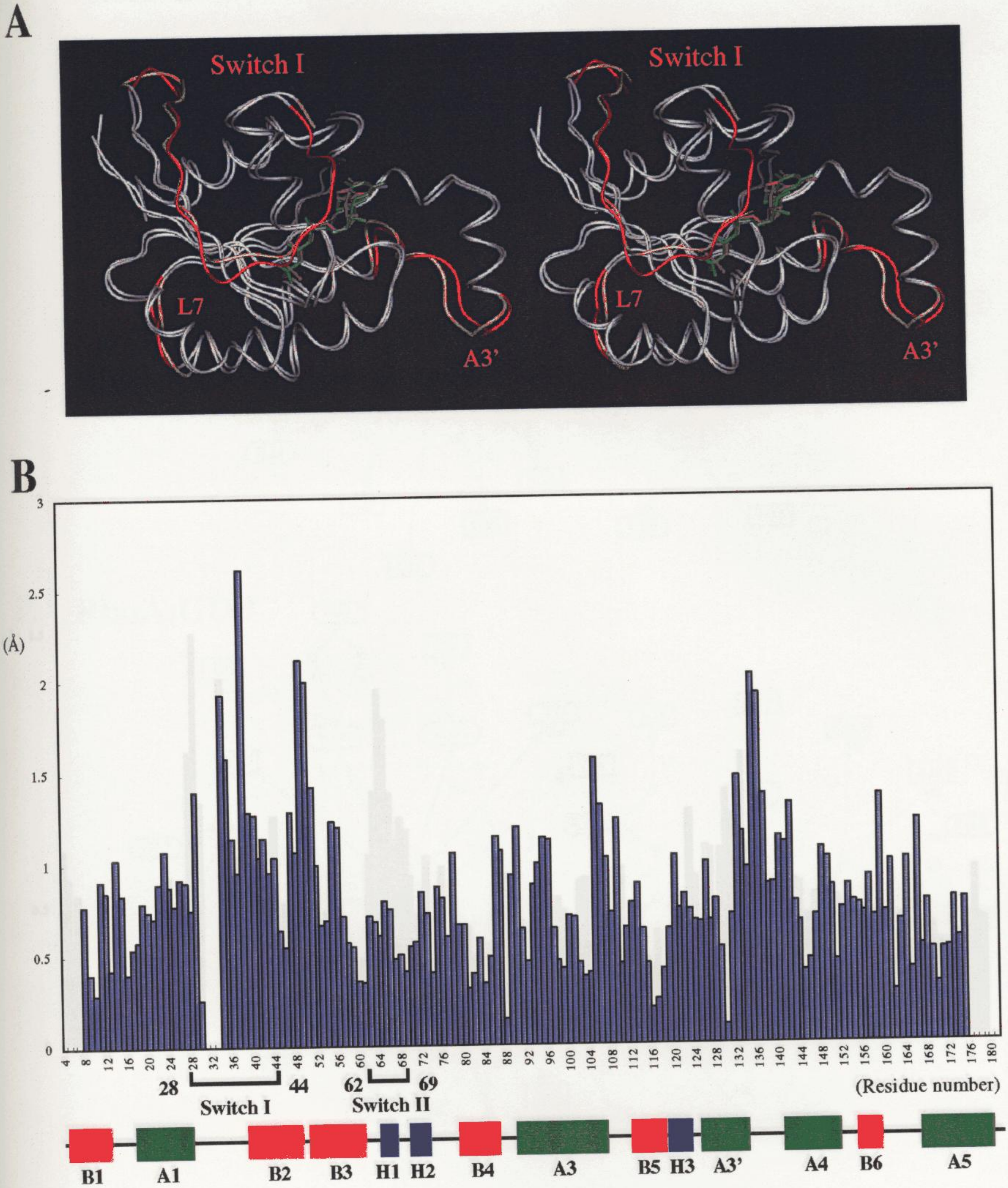

Fig. 11. Structural comparison of RhoA^{V14}-GTPγS with Cdc42-GMP-PNP-rhoGAP.
A, superposition of C$_{\alpha}$-carbon atom tracings of RhoA^{V14} bound to GTPγS (magenta) and Cdc42 bound to GMP-PNP (green) complexed with rhoGAP (chain F of Protein Data Bank code 1AM4; Rittinger *et al.*, 1997) with segments displaying large displacements in red and yellow, respectively. These include switch I and the C-terminal flanking region (residues 29-51 for RhoA), the C-terminal flanking region of the 13-residue insertion (residues 132-142), and the segment L7 (residues 105-109). In Cdc42, residues 31-33 for RhoA are disordered. ***B***, a histogram shows distances between the corresponding C$_{\alpha}$-carbon atoms between RhoA^{V14}-GTPγS and Cdc42-GMP-PNP, with the secondary structure elements of RhoA^{V14} at the bottom.

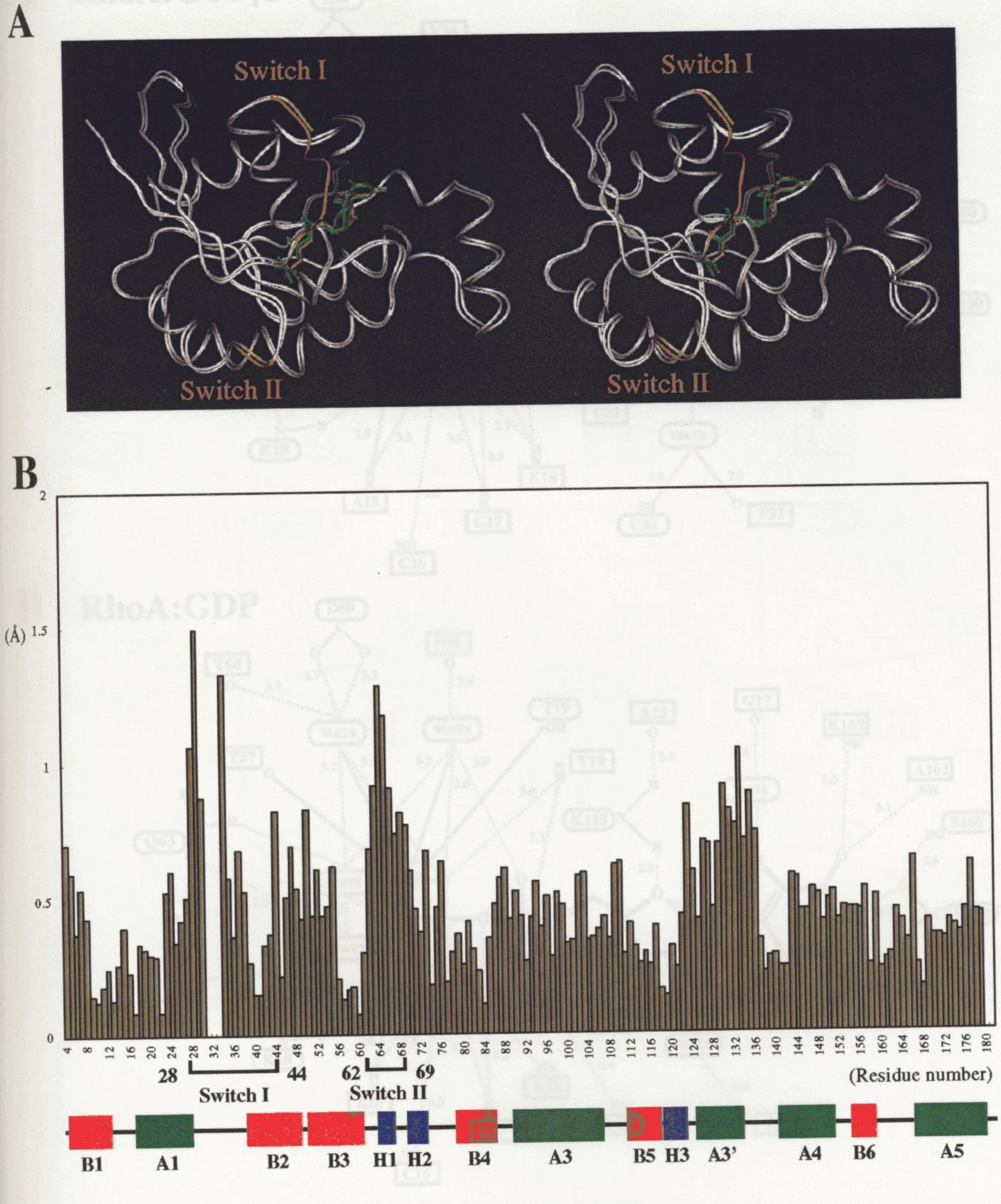

Fig. 12. Structural comparison of RhoA^{V14}-GTPγS with RhoA-GDP-AlF$_4^-$-rhoGAP.
A, superposition of C$_\alpha$-carbon atom tracings of RhoA^{V14} bound to GTPγS (magenta) and RhoA bound to GDP and AlF$_4^-$ (green) complexed with rhoGAP (Protein Data Bank code 1TX4; Rittinger *et al.*, 1997) with segments displaying large displacements in red and yellow, respectively. These include switch I (residues 28-34) and switch II (residues 64, 65). In RhoA-GDP-AlF$_4^-$, residues 31-33 are disordered. ***B***, a histogram shows distances between the corresponding C$_\alpha$-carbon atoms between RhoA^{V14}-GTPγS and RhoA-GDP-AlF$_4^-$, with the secondary structure elements of RhoA^{V14} at the bottom.

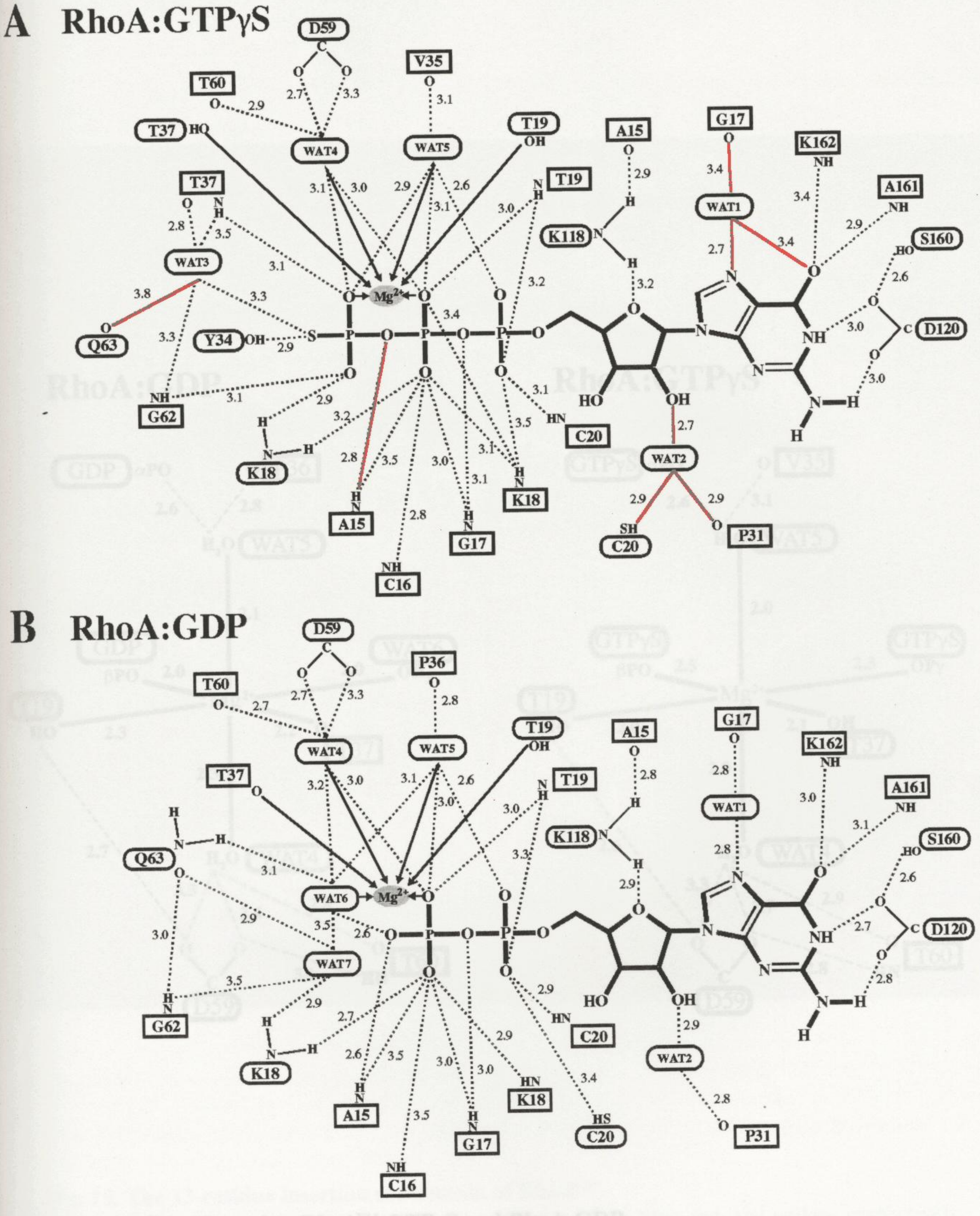
A RhoA:GTPγS
D59
V35
T60
T37
WAT4
WAT5
T19 OH
A15
G17
K162 NH
A161 NH
S160
T37
T19
WAT1
WAT3
K118
Mg2+
Q63
Y34 OH
D120
G62
K18
A15
C20
WAT2
K18
G17
C16
C20
P31
B RhoA:GDP
D59
P36
T60
WAT4
WAT5
T19 OH
A15
G17
K162 NH
T37
T19
WAT1
A161 NH
Q63
K118
S160
WAT6
Mg2+
D120
WAT7
G62
C20
K18
WAT2
A15
K18
G17
C20
P31
C16

Fig. 13. GTPγS and GDP bound to RhoA^{V14}.

A, cartoon shows GTPγS binding to RhoA^{V14} with Mg^{2+} and water molecules. All dashed lines correspond to hydrogen bonding interactions (distance less than 3.5 Å), and the corresponding distances (Å) are indicated. The residues whose main chains participate in the hydrogen bonding are represented by rectangles, and the residues whose side chains participate in the hydrogen bonding are represented by ovals. The coordination bonds to the Mg^{2+} ion are indicated by arrows. The possible hydrogen bond between Gln63 and Wat3 has a longer distance (3.8 Å). The hydrogen bonds observed in the current structure but not in H-Ras are highlighted in red. ***B***, for RhoA-GDP (Wei *et al.*, 1997).

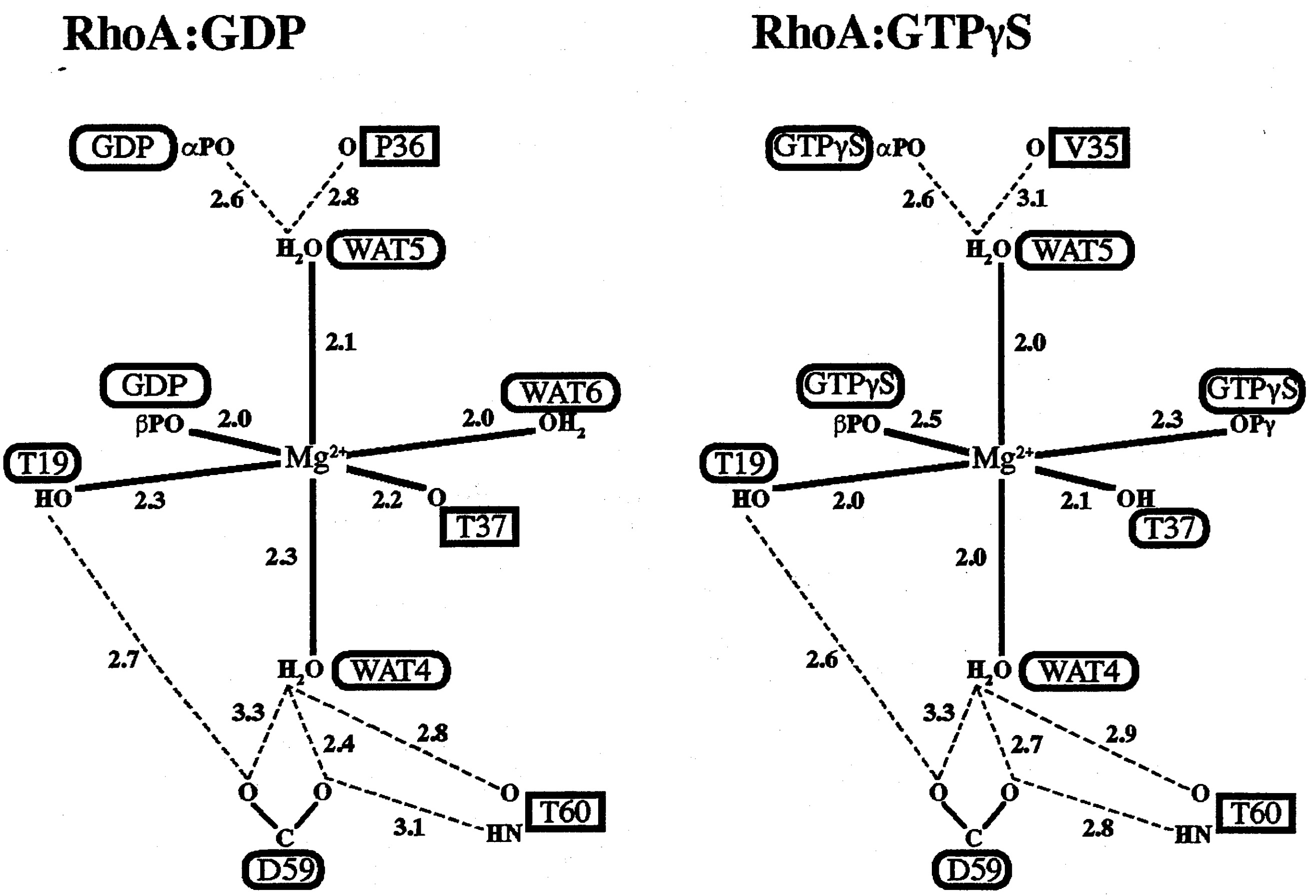
RhoA:GDP

RhoA:GTPγS

GDP
αPO
O
P36
2.6
2.8
H2O
WAT5
2.1
GDP
βPO
2.0
2.0
WAT6
OH2
T19
HO
Mg2+
2.3
2.2
O
T37
2.3
2.7
H2O
WAT4
3.3
2.4
2.8
O
O
O
T60
C
3.1
HN
D59
GTPγS
αPO
O
V35
2.6
3.1
H2O
WAT5
2.0
GTPγS
βPO
2.5
2.3
GTPγS
OPγ
T19
HO
Mg2+
2.0
2.1
OH
T37
2.0
2.6
H2O
WAT4
3.3
2.7
2.9
O
O
O
T60
C
2.8
HN
D59

Fig. 14. Mg^{2+} ion bound to $RhoA^{V14}$-GTPγS and RhoA-GDP.
Cartoons of Mg^{2+} binding to $RhoA^{V14}$-GTPγS (right) and RhoA-GDP (left) are shown. Solid lines indicate the coordination to Mg^{2+} ion. Other symbols are same as Fig. 13.

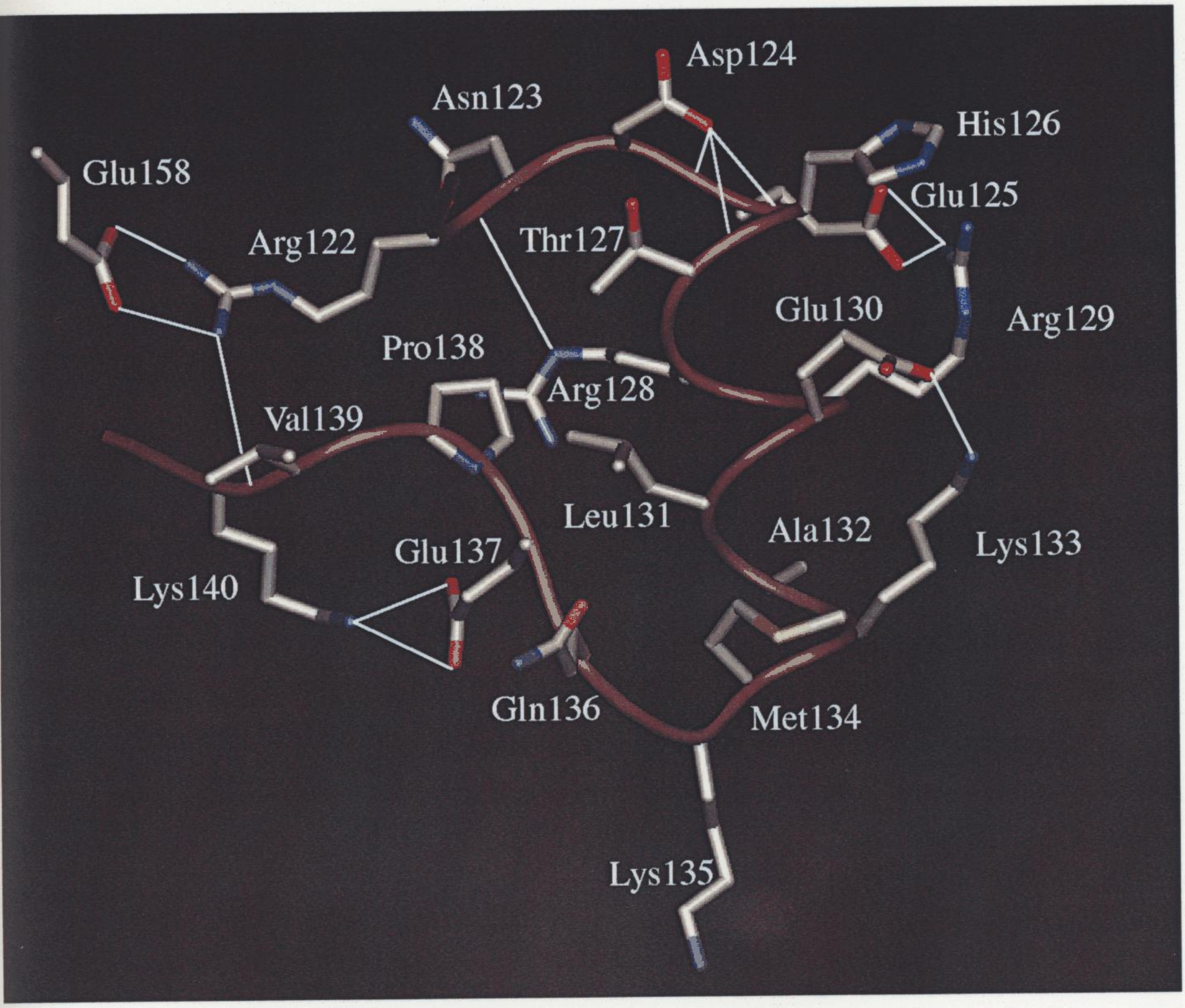
Asp124
Asn123
His126
Glu158
Glu125
Arg122
Thr127
Glu130
Arg129
Pro138
Arg128
Val139
Leu131
Ala132
Lys133
Glu137
Lys140
Gln136
Met134
Lys135

Fig. 15. The 13-residue insertion subdomain of RhoA^{V14}.

The carbon, nitrogen, oxygen, and sulfur atoms are in white, blue, red, and yellow, respectively. The C_α-carbon tracing is in brown. The hydrogen bonds involving the side chains are indicated by thin white lines.

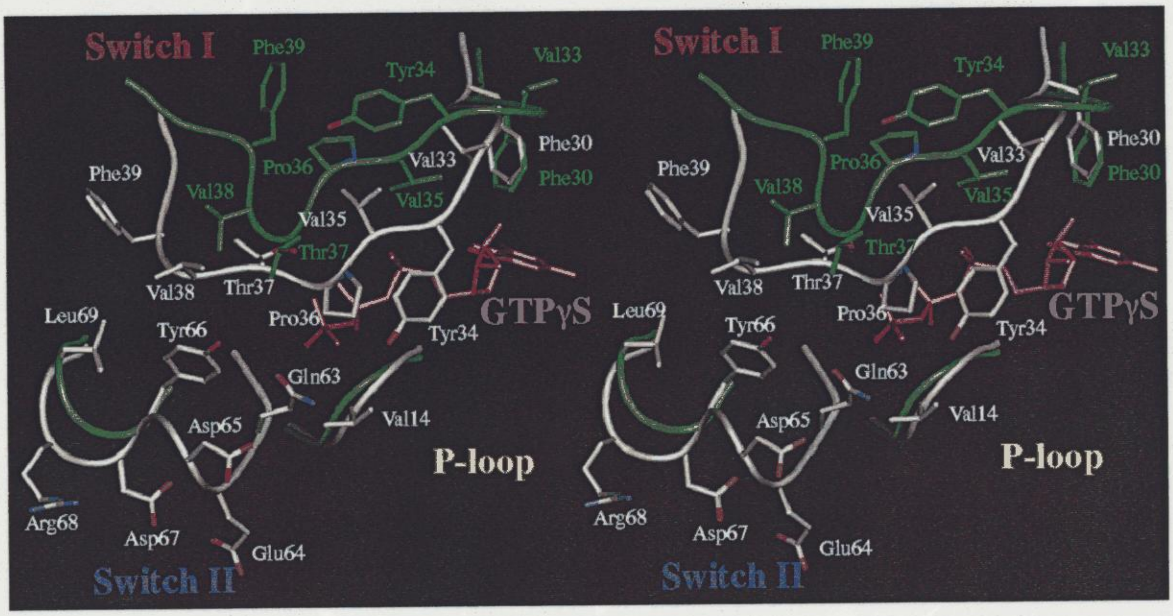
Switch I
Phe39
Tyr34
Val33
Phe30
Phe30
Phe39
Val38
Pro36
Val33
Val35
Val35
Thr37
Val38
Thr37
Pro36
GTPγS
Tyr34
Leu69
Tyr66
Gln63
Asp65
Val14
P-loop
Arg68
Asp67
Glu64
Switch II

Fig. 16. Stereo view of switch regions and phosphate-binding loop of RhoA^{V14}.
Interactions in switches I and II and P-loop regions of RhoA^{V14} (white) bound to GTPγS (magenta). The C_α-carbon atom tracings of the corresponding regions of RhoA-GDP (green), together with the side chains of switch I, are superimposed.

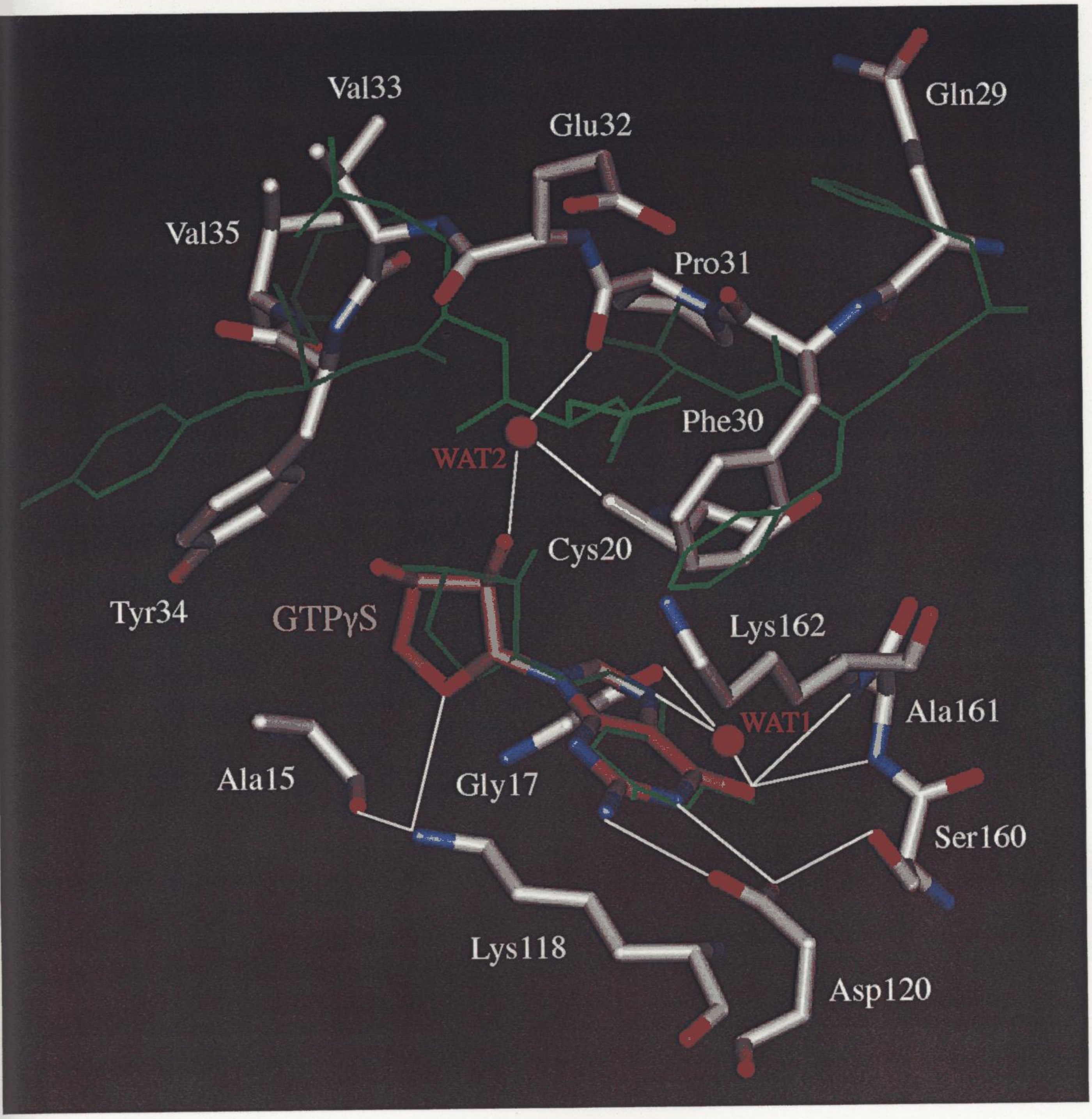
Val33
Glu32
Gln29
Val35
Pro31
Phe30
WAT2
Cys20
Tyr34
GTPγS
Lys162
WAT1
Ala161
Ala15
Gly17
Ser160
Lys118
Asp120

Fig. 17. Recognition of guanosine moiety of GTPγS by RhoA^{V14}.

Part of RhoA^{V14} switch I displays large displacements from the corresponding part of H-Ras^{V12} (green). RhoA^{V14} has two water molecules mediated recognition of guanosine moiety of GTPγS, which are not seen in H-Ras^{V12}-GTP.

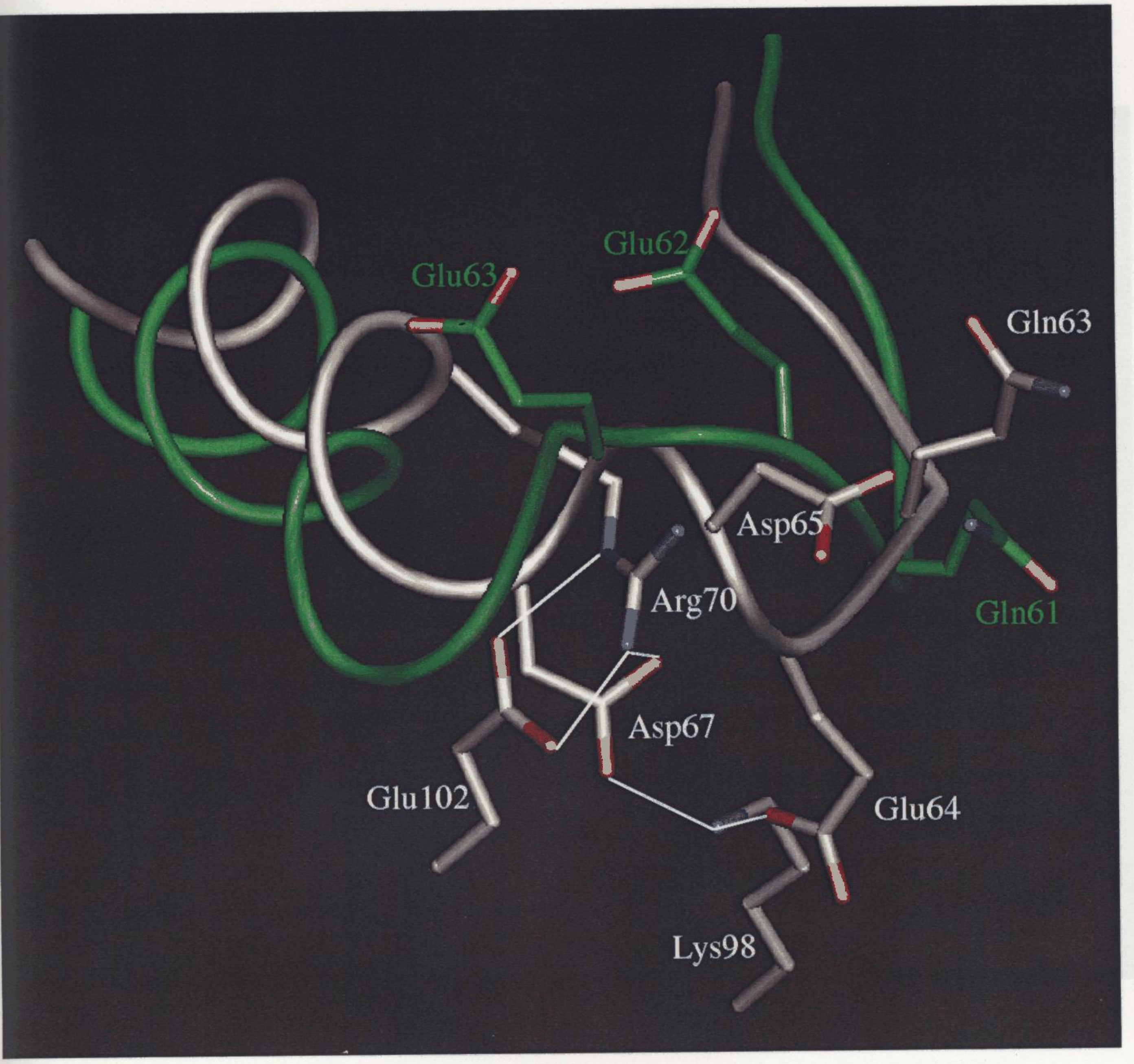
Glu63
Glu62
Gln63
Asp65
Arg70
Gln61
Asp67
Glu102
Glu64
Lys98

Fig. 18. Structural comparison of the switch II of RhoA^{V14}-GTPγS and H-Ras^{V12}-GTP.

Superpositon of C_α-carbon atom tracings of switch II of RhoA^{V14} (white) and H-Ras^{V12} (green). The side chains that stabilize the unique conformation of the RhoA^{V14} switch II are added as well as the functionally important residues. For a clarity, the hydrogen bond between the side chain of Arg70 and the main chain of Ala61 is not shown in this figure.

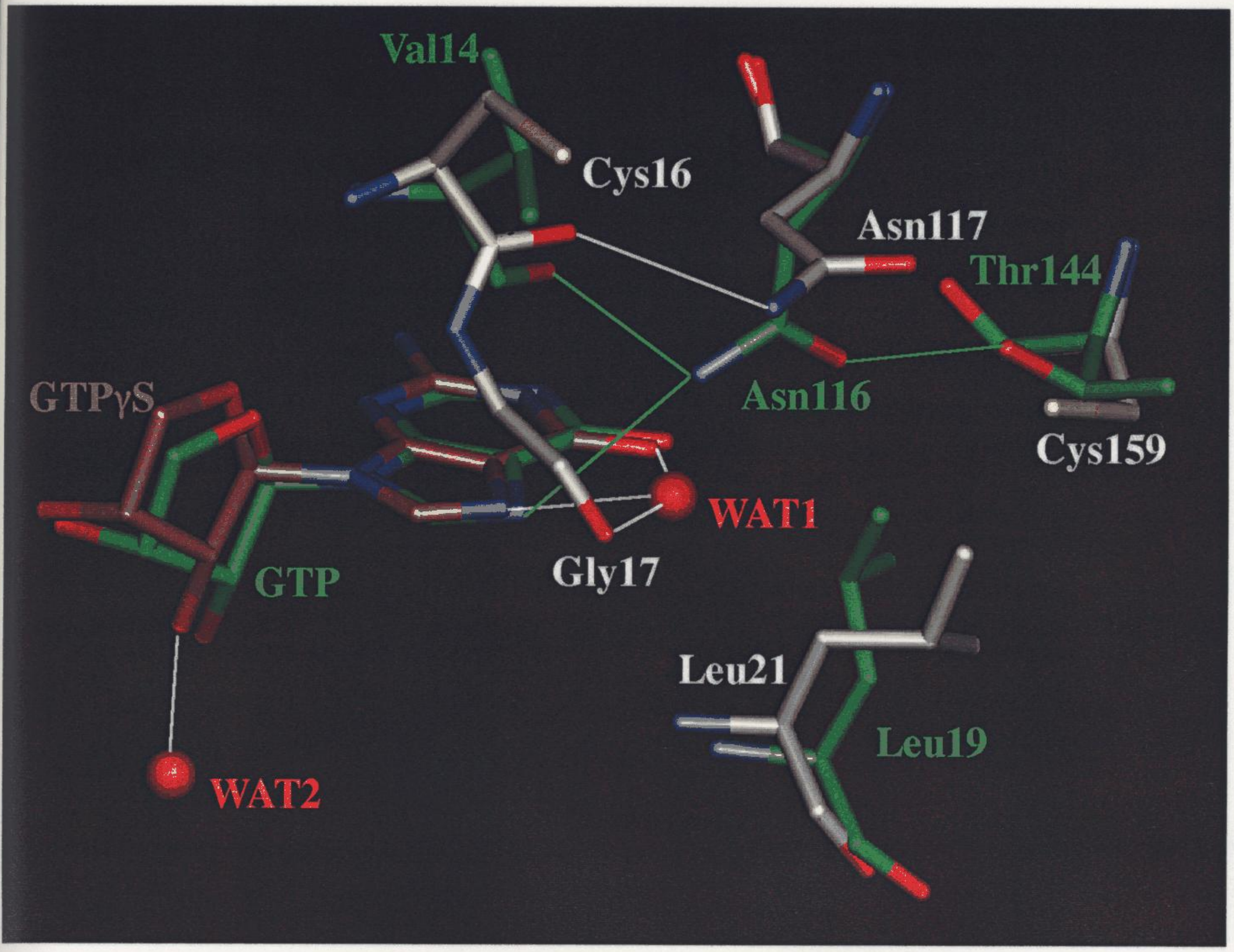
Val14
Cys16
Asn117
Thr144
GTPγS
Asn116
Cys159
WAT1
GTP
Gly17
Leu21
Leu19
WAT2

Fig. 19. Structural difference by Wat1 between RhoA^{V14}-GTPγS and H-Ras^{V12}-GTP.
Rearrangement of the side-chain packing on the guanine recognition site occurs for accomodation of a water molecule (Wat1) of RhoA^{V14}. The corresponding part of H-Ras^{V12} is superimposed with the carbon atoms in green.

Discussion

Modification sites by bacterial toxins

C. botulinum C3 ADP-ribosyltransferase transfers an ADP-ribose moiety of NAD to Asn41 of Rho (Sekine *et al.*, 1989) (Fig. 20). The side-chain of Asn41, which is located at strand B2, forms a hydrogen bond (3.1 Å) to the main-chain carbonyl group of Glu40. This hydrogen bond allows Asn41 to interact with the indole ring of Trp58 of strand B3 (Fig. 21). The distances between the nearest atoms of the indole ring and the carbonyl oxygen atom of the side chain of Asn41 range from 3.3 to 3.5 Å, which indicates the existence of a stacking interaction between them. Because the indole ring is a strong electron-donor, this interaction may help to enhance the nucleophilic properties of the side-chain nitrogen atom of Asn41. It should be noted that the hydrophobic side chains Val38, Phe39, and Val43 are exposed to the solvent region around Ans41, together with Trp58. This unusual feature of the molecular surface may be related to the interaction with C3-like exoenzymes. Asn41 orients the side chain away from the switch I loop. This is consistent with the fact that the ADP-ribosylation on Rho affected neither the GTPγS binding nor its intrinsic GTPase activity. Furthermore, the ADP-ribosylation on Rho did not affect its interaction with rhoGAP (Morii *et al.*, 1991). Recent data using Swiss 3T3 cells indicates that the ADP-ribosylation of Rho enhances its binding PtdIns 4-phosphate 5-kinase and acts as a dominantly negative inhibitor (Ren *et al.*, 1996; Chong *et al.*, 1994). This also suggests that the ADP-ribosylation does not impair the intrinsic properties of the switch I conformation though PtdIns 4-phosphate 5-kinase could bind to the GDP-bound form, and therefore, the binding may be different from those of other effectors that do not bind to the GDP-bound form. Rac and Cdc42 are not subjected to ADP-ribosylation (Just *et al.*, 1992). This may be related to the global conformation of the anti-parallel β-sheet formed by strands B2 and B3 since the sequence of this region of Rho subfamily is conserved but is different from that in the Rac subfamily. On molecular surface around Asn41, Val43 is replaced by Ser/Ala and Glu40 is replaced by Asp in Rac and Cdc42. On the other hand, some sites having the same residues with RhoA show different conformations. In Rac1-GMP-PNP (Hirshberg *et al.*, 1997), Asn39, which corresponds to Asn41 of RhoA, also stacks Trp56 (Trp58 of RhoA), while Phe37, which corresponds to Phe39 of RhoA, burries inside and contacts with the side-chain of Leu69 and the side-chain oxygen atom of Ser71. In Cdc42-GMP-PNP complexed with rhoGAP (Rittinger *et al.*, 1997a), the side-chain carbonyl group of Asn39 makes van der Waals contact with phenol ring of Phe56. Phe37 also burries inside and contacts with the side-chain oxygen atom of Ser71. Therefore, the projected Phe39 of RhoA is only an apparent large difference among the three crystal structures.

Recent biochemical data have shown that Thr37 is glucosylated by the major virulence factors of *C. difficile*, toxin A and B (Just *et al.*, 1994). The glucosylated RhoA induces the disaggregation of actin filaments. It also appears that GDP-bound RhoA is a superior substrate for toxin B to GTP-bound RhoA. This is consistent with the crystal structures: in RhoA-GDP, the side chain of Thr37 does not participate in either Mg^{2+} ion or phosphate binding, whereas it participates in both in the current structure. Since Thr37 orients the side chain inside the loop, its glucosylation must accompany a structural deformation of the loop. This structural change could extend to strand B2. Actually, it has been shown that the glucosylation of Thr37 inhibits ADP-ribosylation by C3-like exoenzyme (Just *et al.*, 1995).

CNFs from *E. coli* and dermonecrotic toxins (DNTs) from *Bordetella* species induce the massive reorganization of the actin cytoskeleton and inhibit cell division, leading multinucleated cells. Recently, CNF1 has been shown to cause the deamidation of Gln63 of RhoA, resulting in a dominantly active form, $RhoA^{E63}$ (Schmidt *et al.*, 1997; Flatau *et al.*, 1997). CNF1 acts preferentially with RhoA but also inhibits the GAP-stimulated GTPase activity of Cdc42 and of Rac at high concentrations. These actions of CNF1 may be related with the unique conformation and/or conformational properties of switch II. The differences in the CNF1 activity on RhoA, Rac, and Cdc42 probably indicate that this toxin may interact with these small GTPases through segments other than switch I, though it remains unclear.

GTP/GDP switching and effector binding

The fundamental mechanism of the molecular switch, which involves the significant conformational changes in switches I and II regions, in signal transduction seems to be common in small GTPases and G_α subunits of trimeric GTPases, as described for H-Ras (Milburn *et al.*, 1990), transducin-α (Lambright *et al.*, 1994), and $G_{i\alpha 1}$ (Mixon *et al.*, 1995) and Rap2A (Cherfils *et al.*, 1997). However, the present RhoA^{V14} structure reveals large conformational deviations from H-Ras^{V12} in the regions containing switches I and II. The structures of two other small GTPases, ADP-ribosylation factor (Arf) (Amor *et al.*, 1994) and Ran (Scheffzek *et al.*, 1995), also showed significant conformational variations in the switch regions, whose structures are also different from those of the present RhoA^{V14}: switch II of Arf forms a long β-strand, and Ran has a completely different orientation of switch II that contains a short β-strand. All these results indicate that small GTPases from different families may have a similar fold but with significant variations in the switch regions.

There are several biochemical data indicating that the switch I region of RhoA is involved in its effector binding. It has been suggested from analyses of the chimeric proteins of Rho and Ras that the switch I region (residue 32-42) is essential for the induction of actin stress fiber formation (Self *et al.*, 1993). Either Cdc42 or Rac shows no significant binding to the target proteins of RhoA, such as Rho-kinase and the others described above. At switch I and its flanking regions of RhoA^{V14}, residues that are exposed to the solvent region are well conserved in the Rho subfamily but are replaced in the Rac subfamily. It is of interest that most of the side chains of these residues protrude onto the same molecular surface (Fig. 22). The double mutant Rap1A (Nassar *et al.*, 1996), which mimics Ras, binds to the Ras-binding domain of c-Raf1 through several residues that are located at the same side of the corresponding molecular surface of RhoA^{V14}. Among them, residues whose side-chains form the specific hydrogen bonds to the

Ras-binding domain are located at the N-terminal half of strand B2. It is notable that most of these residues are replaced by non-conservative, mainly hydrophobic, residues (Val33, Val35, Phe39-Asn41, and Val43) in RhoA^{V14}-GTPγS to form hydrophobic patches on the molecular surface, as described. The electrostatic surface potentials of RhoA^{V14} show several differences from those of H-Ras^{V12} (Fig. 23). Switch I region of H-Ras^{V12} is highly negatively charged, but the corresponding region of RhoA^{V14} is mostly uncharged. These differences suggest that RhoA may binds its effectors proteins through hydrophobic patches on switch I.

In addition to switch I, the second effector site is suggested in the C-terminal two-thirds of the molecule (Self *et al.*, 1993). However, little is currently known about the possible second effector site of RhoA. Recent mutagenesis experiments have indicated that the 13-residue insertion region of Rac1 participates in the interaction with p67phox but not in the interaction with PAK, and a combinational use of the multiple effector-binding sites has therefore been proposed (Freeman *et al.*, 1996). Further experiments have shown the possibility that 13-residue insertion region of Rac1 may bind to the other NADPH oxidase components such as cytochrome b_{558} (Nisimoto *et al.*, 1997). Cdc42 also uses this region to interact with rhoGDI (Wu *et al.*, 1997). Moreover, this region is required for transformation of cells by Rho-related proteins (Wu *et al.*, 1998). Since there are several structural differences in the 13-residue insertion regions among RhoA^{V14}-GTPγS, Rac1-GMP-PNP, and Cdc42-GMP-PNP-rhoGAP, it may be possible that RhoA also utilizes the insertion region in the specific binding with its own effector or regulatory proteins, but this remains to be seen in future experiments. It should be noted that 13-residue insertion region has no significant displacement from that in RhoA-GDP and, therefore, has no switching function between GTP-bound and GDP-bound forms. It is well known that the G_α subunits of trimeric GTPases contain four insertion regions if compared with small GTPases. The 13-residue insertion region of the members of the Rho family corresponds to the third insertion region that forms an additional helix at the N-terminal portion of the segment (Noel *et al.*, 1993), although no homology has been detected between

RhoA and each of G_α subunits and no possible function has been assigned to this insertion region.

Putative effector regions described above have relatively high *B*-factor values (Fig. 24). Such flexibilities are possibly required for binding to the effector proteins. In addition to the switch I and the 13-residue insertion region, switch II and the segment L7 have high *B*-factor values. These regions may also participate in the effector binding.

GEF and GDS binding

GEFs for small GTPases of the Rho family have been identified as Dbl-containing proteins that contain a region with a sequence homology to the *dbl* oncogene product (Cerione *et al.*, 1996). While most of these Dbl-containing proteins can act on multiple members of the Rho family *in vitro*, some have a limited specificity for one type of the GTPases *in vivo*. Among them, Lbc shows selectivity for Rho (Zheng *et al.*, 1995) but Tiam-1 for Rac (Habets *et al.*, 1994) and Cdc24 for Cdc42 (Hart *et al.*, 1991). Analysis of RhoA/Cdc42Hs chimeric proteins has suggested that residues of switch I and switch II are involved in the specific interaction with Lbc (Li *et al.*, 1997). Based on mutation analyses, Lys27, Tyr34, Thr37, and Phe39 in switch I and Asp76 in switch II have been identified as Lbc-sensitive residues. These residues are located at nearly the same side of the molecule, which may form a surface of interaction for Lbc. It is of interest that this surface is almost the same as that for a tentative effector binding (Fig. 22). The side chains of all these residues are highly projected toward the solvent region but Thr37 is buried inside the switch I loop. This might be one reason why the mutation of T37A has an affinity for Lbc comparable with the wild-type RhoA although most of the other mutants failed to associate with Lbc. In contrast, extensive mutations in switch II have been reported to have no significant change in their sensitivity to Lbc. Most of these residues are found on the other side of the molecule or inside the protein. It is notable that the ADP-ribosylated residue by C3-like exoenzymes, Asn41, is also located at this surface and may inhibit the binding to Lbc. There is another protein having guanine nucleotide exchange activity, smgGDS, that has no homology to Cdc25 of yeast (Kaibuchi *et al.*, 1991; Yaku *et al.*, 1994). smgGDS shows wider specificity than Dbl homologues and acts on Ki-Ras, Rap in addition to the Rho family members. Rho seems to interact with smgGDS through its molecular surface containing Asn41 since ADP-ribosylation of Rho by C3-like exoenzymes is reduced the interaction in the presence of smgGDS (Kikuchi *et al.*, 1992).

GDI binding

In addition to inhibiting nucleotide dissociation, GDIs mediate partitioning their cognate small GTPases between the membrane and the cytosol (Araki *et al.*, 1990). rhoGDI inhibits the guanine nucleotide exchange of all members of the Rho family. Recent structural studies have suggested that rhoGDI binds to the cognate GTPases via an immunoglobulin-like domain that has a hydrophobic pocket for binding to the C-terminal isoprenyl group (Gosser *et al.*, 1997; Keep *et al.*, 1997). Although this immunoglobulin-like domain has little effect on the rate of nucleotide dissociation from the GTPases, it has been suggested that this binding directs the flexible N-terminal arm of rhoGDI to GTPases, resulting in the inhibition of nucleotide exchange. It is of interest to question how the N-terminal arm interacts with GTPases because the C-terminus having the isoprenyl group is located on the molecular surface of the GTPases opposite to the nucleotide binding surface. It has been reported that GDI effectively prevents ADP-ribosylation by C3-like exoenzyme and the nucleotide-exchange activity of smgGDS (Kikuchi *et al.*, 1992). Furthermore, the nucleotide-exchange activity of Dbl also was remarkably reduced (Yaku *et al.*, 1994). Taken together, these results suggest that the N-terminal arm of rhoGDI may interact with GTPases on the molecular surface, which has residues interact with GEF and GDS as well as C3-like exoenzymes (Fig. 19). This hypothesis provides a framework for analyzing the interactions of rhoGDI, GEF, and GDS with RhoA.

Effects of the γ-sulfur atom and the G14V mutation on the GTPase activity

The GTPγS molecule exhibits its resistance to hydrolysis, which is conferred by the γ-thiophosphorothioate. In the present structure, the γ-thiophosphate turns the sulfur-phosphorus bond toward Gln63 and positions the γ-sulfur atom to come into contact with the putative nucleophilic water molecule. Therefore, the bulky sulfur atom, which has a van der waals radius (1.8 Å) much larger than that of the oxygen atom (1.4 Å), sterically shields the phosphorus atom from the close approach of the nucleophilic water molecule and could interfere with the stabilization of the transition state by Gln63. The γ-sulfur atom could also interfere with the stabilization of the transition state by Arg residue from GAP (Rittinger *et al.*, 1997b). Similar mechanisms for the resistance of the GTPγS molecule to hydrolysis, which is conferred by the γ-thiophosphorothioate, are possible for transducin-α and $G_{i\alpha 1}$. Based on the crystal structure of transducin-α complexed with GTPγS, it has also been pointed out that Arg174, which is a key residue stabilizing the transition state, prevents the thiophophate from reaching the transition state, due to a steric clash between the firmly anchored guanidino group and the sulfur atom (Noel *et al.*, 1993).

It has been suggested that the role of the key Gln residue (Gln63 of RhoA) is to stabilize the transition state by direct hydrogen bond doubly bonded to the γ-phosphate and the putative nucleophilic water molecule. The transition state should induce conformational changes around the active site of the current structure since the present conformation of Gln63 directs the side-chain carbonyl group toward the nucleolytic water molecule (3.8 Å) but also positions the side-chain amide group away from the phosphate. The γ-sulfur atom of the phosphate is closest to the side-chain amide group of Gln63, as described above, but the distance between them is more than 5 Å. The contacts of the branched side chain of Val14 with the N-terminus of switch II seem to push Gln63 away from the γ-phosphate group and reduce the conformational flexibility of the side-chain of Gln63. Actually, the Cγ carbon atoms of Val14 and Gln63 have a contact of 3.6 Å. Any rotation around the side-chain torsions of Gln63 could not bring the side-chain amide group to a position close enough to interact with the γ-sulfur atom because of the steric hindrance of the bulky side chain of Val14. We postulate that these steric effects are a possible means of inhibiting GTP hydrolysis by the dominantly active mutation V14 of RhoA. Thus, the mechanism of dominant activation by the G14V mutation of RhoA seems to be similar to that of G12V of H-Ras even though the conformations of switches I and II are quite different.

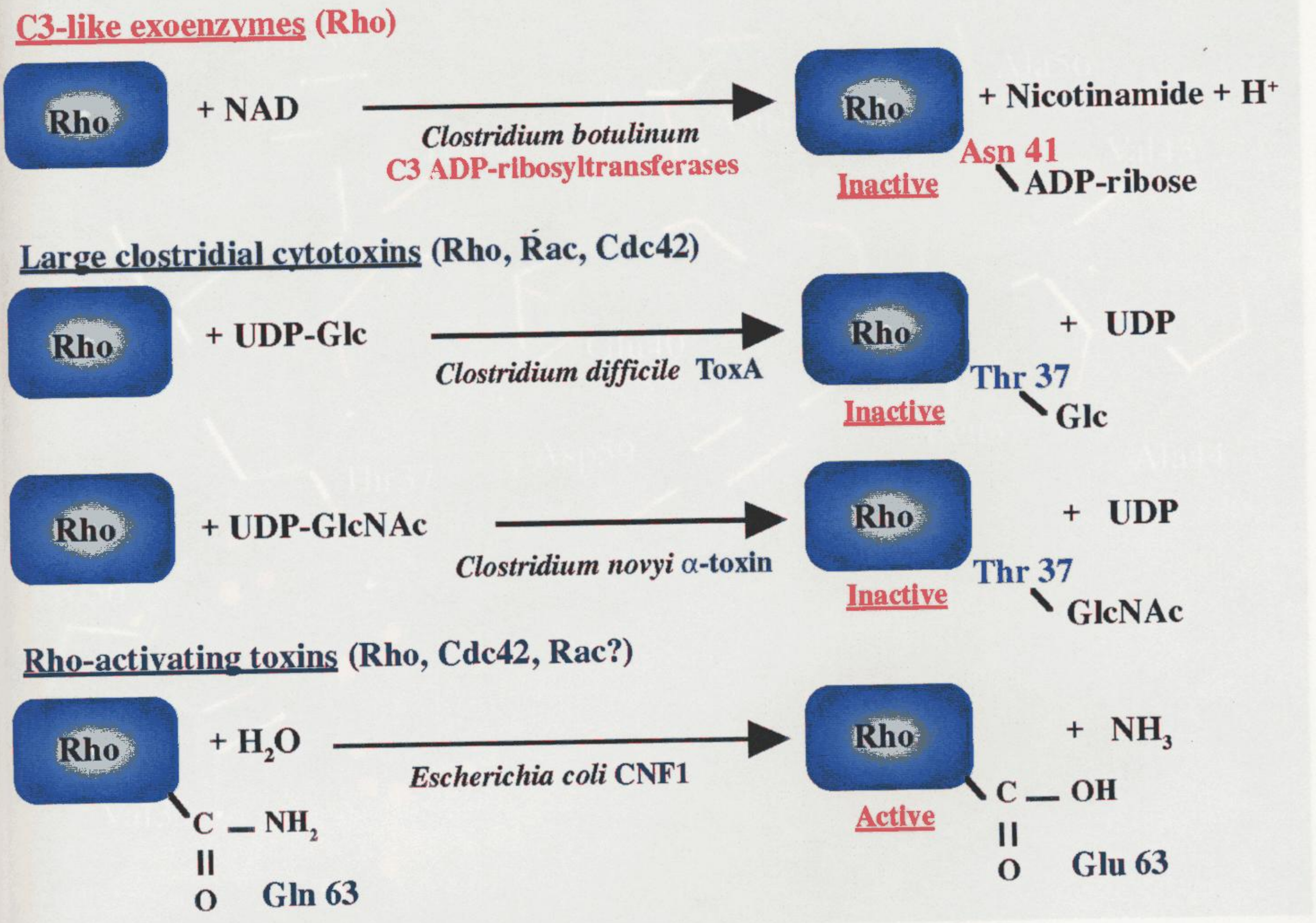
C3-like exoenzymes (Rho)
Rho
+ NAD
Clostridium botulinum
C3 ADP-ribosyltransferases
Rho
+ Nicotinamide + H+
Asn 41
ADP-ribose
Inactive
Large clostridial cytotoxins (Rho, Rac, Cdc42)
Rho
+ UDP-Glc
Clostridium difficile ToxA
Rho
+ UDP
Thr 37
Glc
Inactive
Rho
+ UDP-GlcNAc
Clostridium novyi α-toxin
Rho
+ UDP
Thr 37
GlcNAc
Inactive
Rho-activating toxins (Rho, Cdc42, Rac?)
Rho
+ H2O
C — NH2
O
Gln 63
Escherichia coli CNF1
Rho
+ NH3
C — OH
O
Glu 63
Active

Fig. 20. Modification sites by bacterial toxins on Rho family GTPases.
A cartoon summarizes the chemical reactions at the modification sites by bacterial toxins on the Rho family GTPases (Aktories, 1997).

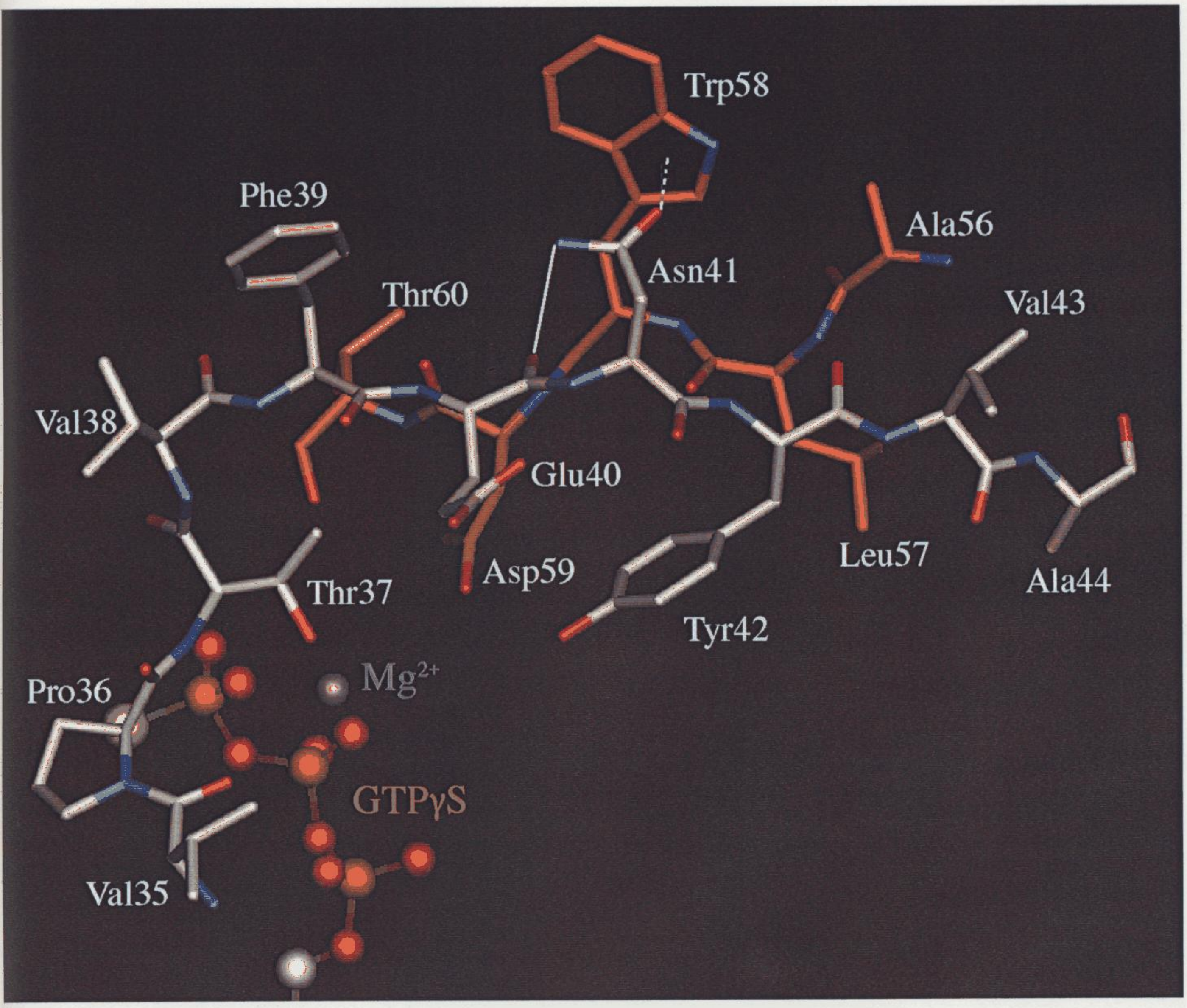
Trp58
Phe39
Ala56
Asn41
Thr60
Val43
Val38
Glu40
Leu57
Asp59
Thr37
Ala44
Tyr42
Mg2+
Pro36
GTPγS
Val35

Fig. 21. Modification sites by bacterial toxins on RhoA^{V14}.

Modification sites by bacterial toxins located at C-terminus of switch I and part of β-sheet B2 (white) - B3 (brown). The stacking interaction between the side-chain carbonyl group of Asn41 and the indole ring of Trp58 is indicated by a broken line. The target residue, Thr37, for glucosylation by large closteidal cytotoxins is located at the N-terminus of switch I. The Mg^{2+} ion and the triphosphate group of GTPγS is shown with a ball-and-stick model.

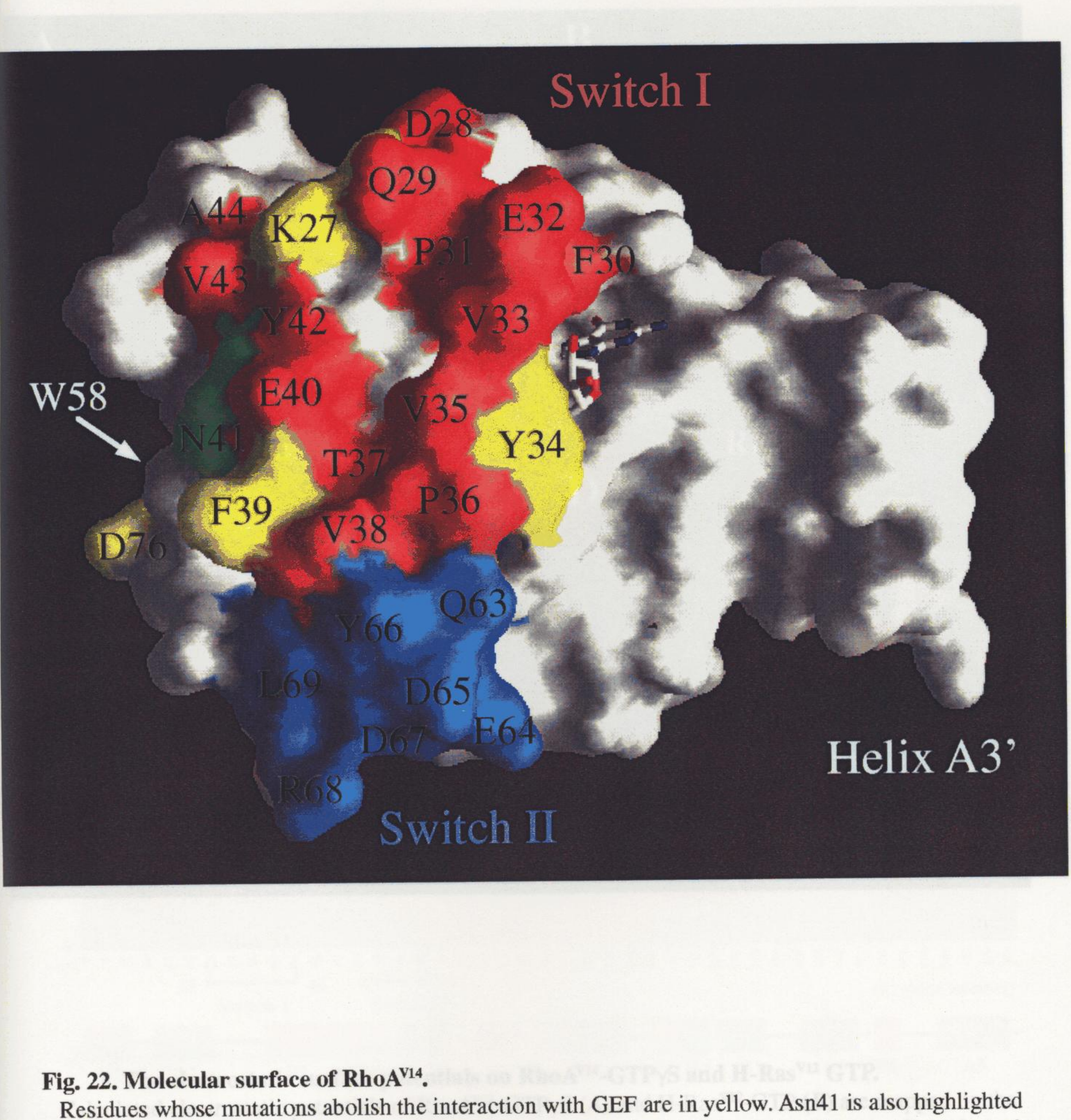
Switch I
D28
Q29
A44
K27
E32
P31
F30
V43
Y42
V33
W58
E40
V35
N41
Y34
T37
F39
P36
D76
V38
Q63
Y66
L69
D65
E64
D67
R68
Helix A3'
Switch II

Fig. 22. Molecular surface of RhoA^{V14}.

Residues whose mutations abolish the interaction with GEF are in yellow. Asn41 is also highlighted in green. Switches I and II are shown in red and blue, respectively. This surface also contains most of the residues corresponding to the effector-binding residues as seen in the complex between the Ras-binding domain of Raf1 and a double mutant Rap1A (E30D/K31E), which mimics Ras.

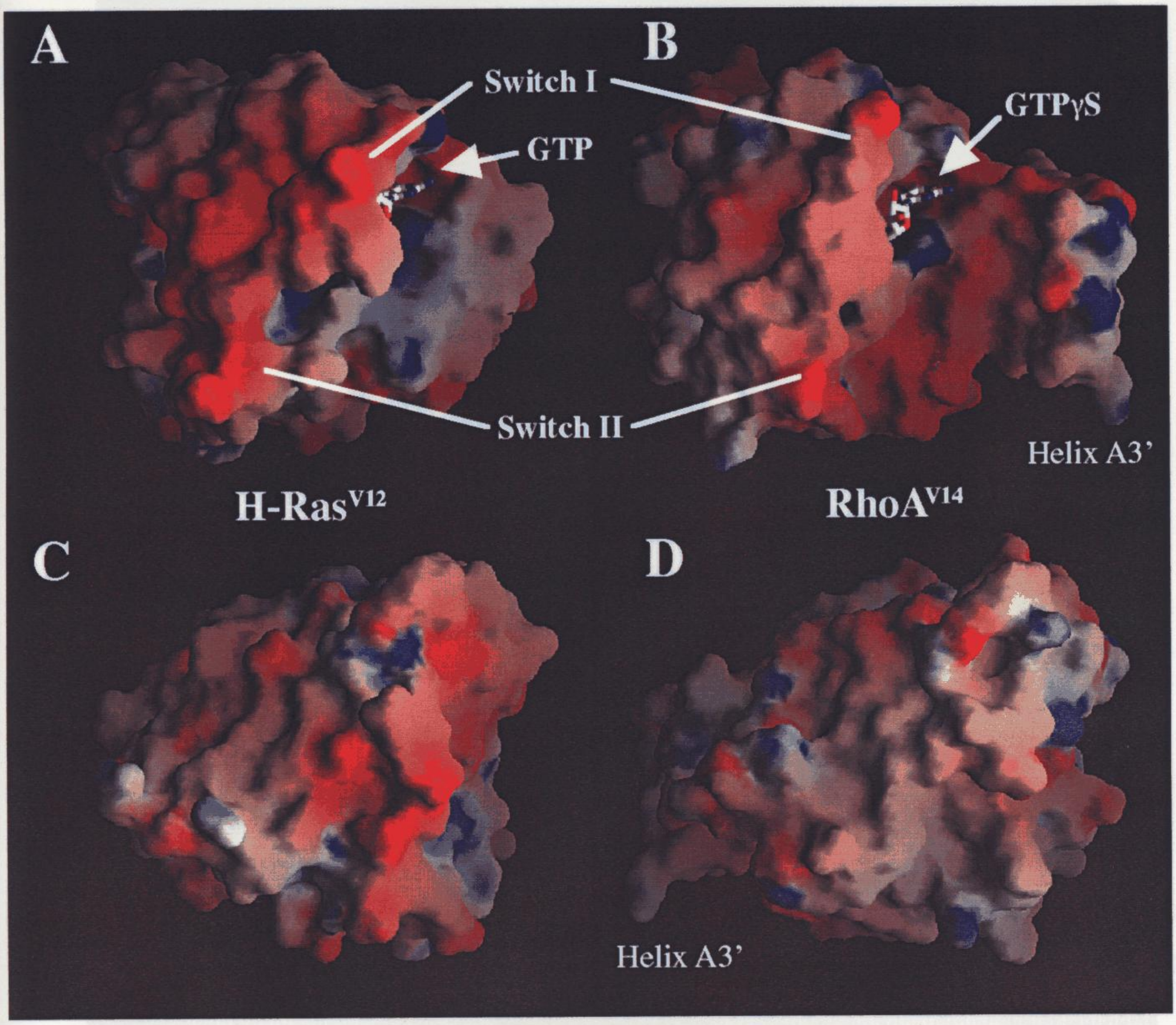
A
B
Switch I
GTP
GTPγS
Switch II
Helix A3'
H-Ras^V12
RhoA^V14
C
D
Helix A3'

Fig. 23. The electrostatic surface potentials on RhoA^{V14}-GTPγS and H-Ras^{V12} GTP.

Calculated electrostatic potentials of RhoA^{V14}-GTPγS (*A*) and H-Ras^{V12}-GTP (***B***) are mapped on the molecular surfaces. Positive charges in blue and negative charges in red. ***C*** and ***D***, views from the very opposite side. H-Ras^{V12} has highly negatively charged region on switch I, while not in RhoA^{V14}.

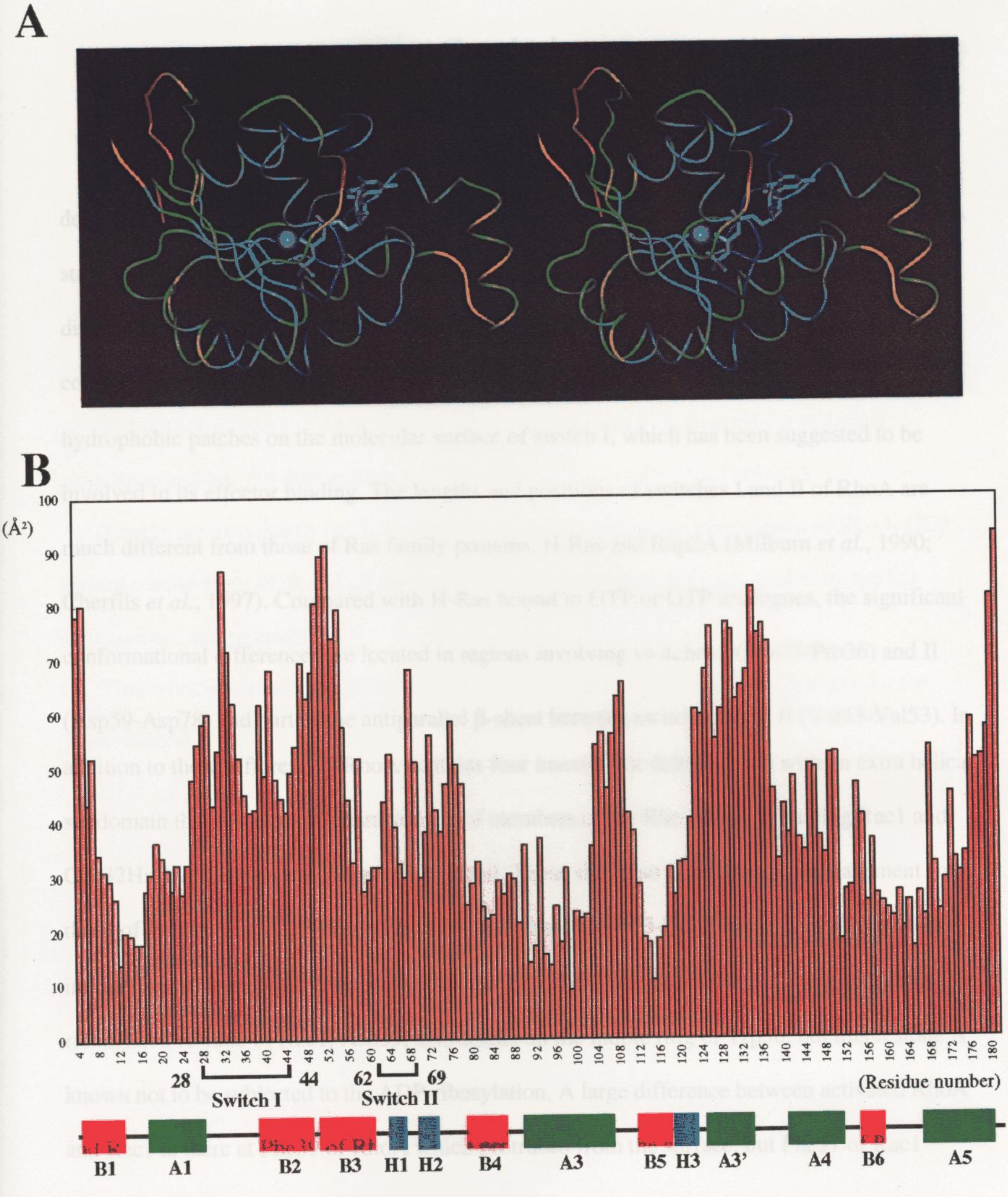

Fig. 24. Residual averaged *B*-factors of RhoA^{V14}-GTPγS.

A, residual averaged *B*-factors are ploted on C$_{\alpha}$-carbon atom tracings of RhoA^{V14} bound to GTPγS and Mg^{2+} ion. Residues having low *B*-factor values are painted blue and gradually shifted to red corresponding to increase of *B*-factor value. The N-terminus, the C-terminus, the region from switches I to II (residues 26-78), the segment L7 (residues 103-112), and the 13-residue insertion (residues 123-137) have relatively high *B*-factor values. Large sphere is a Mg^{2+} ion. Both GTPγS and Mg^{2+} ion have almost same *B*-factor values of about 30 Å^2. *B*, a histogram shows *B*-factor values of the corresponding residues, with the secondary structure elements of RhoA^{V14} at the bottom.

Conclusion

The crystal structure of RhoA^{V14} complexed with a GTPγS and a Mg^{2+} ion was determined at 2.4 Å resolution, with an *R*-factor of 19.5 % and a free *R*-factor of 26.8 %. This structure has a similar fold to RhoA-GDP (Wei *et al.*,1997), but shows large conformational differences localized in switches I (Asp28-Ala44) and II (Gly62-Arg68). No significant conformational change exists in the 13-residue insertion region. These changes produce hydrophobic patches on the molecular surface of switch I, which has been suggested to be involved in its effector binding. The lengths and positions of switches I and II of RhoA are much different from those of Ras family proteins, H-Ras and Rap2A (Milburn *et al.*, 1990; Cherfils *et al.*, 1997). Compared with H-Ras bound to GTP or GTP analogues, the significant conformational differences are located in regions involving switches I (Lys27-Pro36) and II (Asp59-Asp78) and part of the antiparallel β-sheet between switches I and II (Val43-Val53). In addition to these differences, RhoA contains four insertion or deletion sites with an extra helical subdomain that seems to be characteristic of members of the Rho family, including Rac1 and Cdc42Hs, but with several variations in detail. These sites also display large displacement from those of H-Ras. The ADP-ribosylation residue, Asn41, by C3-like exoenzymes stacks on the indole ring of Trp58 with a hydrogen bond to the main chain of Glu40. The corresponding ribosylated residue of Rac1, Asn39, also stacks on the indole ring of Trp56, but this residue is known not to be subjected to the ADP-ribosylation. A large difference between activated RhoA and Rac1 is there at Phe39 of RhoA which protrudes from the surface, but Phe37 of Rac1 burries inside the protein. The recognitions of GTPγS and Mg^{2+} ion by RhoA are almost same as H-Ras-GMP-PNP (Pai *et al.*, 1990), but in the recognition of the guanosine moiety of GTPγS contains water-mediated hydrogen bonds, which seems to be common in the Rho family GTPases. These structural differences provide an insight into specific interaction sites with the effectors, as well as with modulators such as GEF and GDI.

Acknowledgements

The present studies have been performed under the direction of Professor Toshio Hakoshima (Division of structural biology, Nara Institute of Science and Technology).

The author wishes to express his sincere gratitude to Ms. S. Muraguchi, Dr. M. Kato, Dr. T. Shimizu, Dr. M. Shirakawa (Division of structural biology), Dr. S. Kuroda, and Dr. K. Kaibuchi (Division of signal transduction).

The author thanks to Drs. S. Takayama, F.-S. Che, and T. Katsuragi for technical assistance and helpful discussions.

Thanks are also due to Dr. Z. S. Derewenda for providing the coordinates of RhoA-GDP before release from PDB and all the members of the labolatory for their kind help, usefull discussions, and patience.

This work was partly supported by a reserch fellowship from the Japan Society for the Promotion of Science to the author.

References

Abo, A., Pick, E., Hall, A., Totty, N., Teahan, C. G., and Segal, A. W. (1991). Activation of the NADPH oxidase involves the small GTP-binding protein p21rac1. *Nature* **353**, 668-670

Aktories, K. (1997). Rho proteins: targets for bacterial toxins. *Trends Microbiol.* **5**, 282-287

Amano, M., Ito, M., Kimura, K., Fukata, Y., Chihara, K., Nakano, T., Matsuura, Y., and Kaibuchi, K. (1996a). Phosphorylation and activation of myosin by Rho-associated kinase (Rho-kinase). *J. Biol. Chem.* **271**, 20246-20249

Amano, M., Mukai, H., Ono, Y., Chihara, K., Matsui, T., Hamajima, Y., Okawa, K., Iwamatsu, A., and Kaibuchi, K. (1996b). Identification of a putative target for Rho as the serine-threonine kinase protein kinase N. *Science* **271**, 648-650

Amano, M., Chihara, K., Kimura, K., Fukata, Y., Nakamura, N., Matsuura, Y., and Kaibuchi, K. (1997). Formation of actin stress fibers and focal adhesions enhanced by Rho-kinase. *Science* **275**, 1308-1311

Amano, M., Chihara, K., Nakamura, N., Fukata, Y., Yano, T., Shibata, M., Ikebe, M., and Kaibuchi, K. (1998). Myosin II activation promotes neurite retraction during the action of Rho and Rho-kinase. *Genes Cells* **3**, 177-188

Amor, J. C., Harrison, D. H., Kahn, R. A., and Ringe, D. (1994). Structure of the human ADP-ribosylation factor 1 complexed with GDP. *Nature* **372**, 704-708

Araki, S., Kikuchi, A., Hata, Y., Isomura, M., and Takai, Y. (1990). Regulation of reversible binding of smg p25A, a ras p21-like GTP-binding protein, to synaptic plasma membranes and vesicles by its specific regulatory protein, GDP dissociation inhibitor. *J. Biol. Chem.* **265**, 13007-13015

Berchtold, H., Reshetnikova, L., Reiserm, C. O. A., Schirmer, N. K., Spinzl, M., and Hillgenfeld, R. (1993). Crystal structure of active elongation factor Tu reveals major domain rearrangements. *Nature* **365**, 126-132

Brünger, A. T., Kuriyan, J., and Karplus, M. (1990). Slow-cooling protocols for crystallographic refinement by simulated annealing. *Acta Crystallogr. Sec. A* **46**, 585-593

Brünger, A. T. (1996). Free R value: a novel statistical quantity for assessing the accuracy of crystal structure. *Nature* **355**, 472-475

Cerione, R. A., and Zheng, Y. (1996). The Dbl family of oncogenes. *Curr. Biol.* **8**, 216-222

Cherfils, J., Menetrey, J., Le Bras, G., Le Bras, Janoueix-Lerosey, I., de Gunzburg, J., Garel, J.-R., and Auzat, I. (1997). Crystal structures of the small G protein Rap2A in complex with its substrate GTP, with GDP and with GTPgammaS. *EMBO J.* **16**, 5582-5591

Chihara, K., Amano, M., Nakamura, N., Yano, T., Shibata, M., Tokui, T., Ichikawa, H., Ikebe, R., Ikebe, M., and Kaibuchi, K. (1997). Cytoskeletal rearrangements and transcriptonal activation of c-fos serum response element by Rho-kinase. *J. Biol. Chem.* **272**, 25121-25127

Chong, L. D., Traynor-Kaplan, A., Bokoch, G. M., and Schwartz, M. A. (1994). The small GTP-binding protein Rho regulates a phosphatidylinositol 4-phosphate 5-kinase in mammalian cells. *Cell* **79**, 507-513

Coleman, D. E., Berghuis, A. M., Lee, E., Linder, M. E., Gilman, A. G., and Sprang, S. R. (1994). Structures of active conformations of Gi alpha 1 and the mechanism of GTP hydrolysis. *Science* **265**, 1405-1412

Cowtan, K. D., and Main, P. (1996). Phase combination and cross valedation in iterated density-modification calculations. *Acta Crystallogr. Sec. D* **52**, 43-48

Crowther, R. A., and Blow, D. M. (1967). A method of positioning a known molecule in an unknown crystal structure. *Acta Crystallogr.* **23**, 544-548

Crowther, R. A. (1972). in: *The molecular Replacement Method*, pp.173-178; edited Rossmann, M. G., ed. Gordon and Breach, New York

Der, C. J., Finkel, T., and Cooper, G. M. (1986). Biological and biochemical properties of human rasH genes mutated at codon 61. *Cell* **44**, 167-176

Fabian, J. R., Vojtek, A. B., Cooper, J. A., and Morrison, D. K. (1994). A single amino acid change in Raf-1 inhibits Ras binding and alters Raf-1 function. *Proc. Acad. Natl. Sci. U. S. A.* **91**, 5982-5986

Feltham, J. L., Dötsch, V., Raza, S., Manor, D., Cerione, R. A., Sutcliffe, M. J., Wagner, G., and Oswald, R. E. (1997). Definition of the switch surface in the solution structure of Cdc42Hs. *Biochem.* **36**, 8755-8766

Flatau, G., Lemichez, E., Gauthier, M., Chardin, P., Paris, S., Florentini, C., and Baquit, P. (1997). Toxin-induced activation of the G protein p21 Rho by deamidation of glutamine. *Nature* **387**, 729-733

Freeman, J. L., Abo, A., and Lambeth, J. D. (1996). Rac "insert region" is a novel effector region that is implicated in the activation of NADPH oxidase, but not PAK65. *J. Biol. Chem.* **271**, 19794-19801

Fujisawa, K., Fujita, A., Ishizaki, T., Saito, Y., and Narumiya, S. (1996). Identification of the Rho-binding domain of p160ROCK, a Rho-associated coiled-coil containing protein kinase. *J. Biol. Chem.* **271**, 23022-23028

Fujisawa, K., Madaule, P., Ishizaki, T., Watanabe, G., Bito, H., Saito, Y., Hall, A., and Narumiya, S. (1997). Different regions of Rho determine Rho-selective binding of differnt classes of Rho target molecules. *J. Biol. Chem.* **273**, 18943-18949

Gosser, Y. Q., Nomanbhoy, T. K., Aghazadeh, B., Manor, D., Combs, C., Cerione, R. A., and Rosen, M. K. (1997). C-terminal binding domain of Rho GDP-dissociation inhibitor directs N-terminal inhibitory peptide to GTPases. *Nature* **387**, 814-819

Habets, G. G., Scholtes, E. H., Zuydgeest, D., van der Kammen, R. A., Stam, J. C., Berns, A., and Collard, J. G. (1994). Identification of an invasion-inducing gene, Tiam-1, that encodes a protein with homology to GDP-GTP exchangers for Rho-like proteins. *Cell* **77**, 537-549

Hart, M. J., Eva, A., Evans, T., Aaronson, S. A., and Cerione, R. A. (1991). Catalysis of guanine nucleotide exchange on the CDC42Hs protein by the dbl oncogene product. *Nature* **354**, 311-314

Hill, C. S., Wynne, J., and Treisman, R. (1995). The Rho family GTPases RhoA, Rac1, and CDC42Hs reglate transcriptional activation by SRF. *Cell* **81**, 1159-1170

Hirshberg, M., Stockley, R. W., Dodson, G., and Webb, M. R. (1997). The crystal structure of human rac1, a member of the rho-family complexed with a GTP analogue. *Nat. Struct. Biol.* **4**, 147-152

Ihara, K., Muraguchi, S., Kato, M., Shimizu, T., Shirakawa, M., Kuroda, S., Kaibuchi, K., and Hakoshima, T. (1998). Crystal structure of human RhoA in a dominantly active form complexed with a GTP analogue. *J. Biol. Chem.* **273**, 9656-9666.

Ishizaki, T., Maekawa, M., Fujisawa, K., Okawa, K., Iwamatsu, A., Fujita, A., Watanabe, N., Saito, Y., Kakizuka, A., Morii, N., and Narumiya, S. (1996). The small GTP-binding protein Rho binds to and activates a 160 kDa Ser/Thr protein kinase homologous to myotonic dystrophy kinase. *EMBO J.* **15**, 1885-1893

Ishizaki, T., Naito, M., Fujisawa, K., Maekawa, M., Watanabe, N., Saito, Y., and Narumiya, S. (1997). p160ROCK, a Rho-associated coiled-coil forming protein kinase, works downstream of Rho and induces focal adhesions. *FEBS Lett.* **404**, 118-124

Jones, T. A., Zou, J. Y., Cowan, S. W., and Kjeldgaard, M. (1991). Improved methods for binding protein models in electron density maps and the location of errors in these models. *Acta Crystallogr. Sec. A* **47**, 110-119

Just, I., Mohr, C., Schallehn, G., Menard, L., Didsbury, J. R., Vandekerckhove, J., van Damme, J., and Aktories, K. (1992). Purification and characterization of an ADP-ribosyltransf erase produced by Clostridium limosum. *J. Biol. Chem.* **267**, 10247-10280

Just, I., Richter, H. P., Prepens, U., von Eichel-Streiber, C., and Aktories, K. (1994). Probing the action of Clostridium difficile toxin B in Xenopus laevis oocytes. *J. Cell Sci.* **107**, 1653-1659

Just, I., Selzer, J., Wilm, M., von Eichel-Streiber, C., Mann, M., and Aktories, K. (1995). Glucosylation of Rho proteins by Clostridium difficile toxin B. *Nature* **375**, 500-503

Kaibuchi, K., Mizuno, T., Fujioka, H., Yamamoto, T., Kishi, K., Fukumoto, Y., Hori, Y., and Takai, Y. (1991). Molecular cloning of the cDNA for stimulatory GDP/GTP exchange protein for smg p21s (ras p21-like small GTP-binding proteins) and characterization of stimulatory GDP/GTP exchange protein. *Mol. Cell. Biol.* **11**, 2873-2880

Keep, N. H., Barnes, M., Barsukov, I., Badii, R., Lian, L. Y., Segal, A. W., Moody, P. C., and Roberts, G. C. (1997). A modulator of rho family G proteins, rhoGDI, binds these G proteins via an immunoglobulin-like domain and a flexible N-terminal arm. *Structure* **5**, 623-633

Kikuchi, K., Kuroda, S., Sasaki, T., Kotani, K., Hirata, K., Katayama, M., and Takai, Y. (1992). Functional interactions of stimulatory and inhibitory GDP/GTP exchange proteins and their common substrate small GTP-binding protein. *J. Biol. Chem.* **267**, 14611-14615

Kimura, K., Ito, M., Amano, M., Chihara, K., Fukata, Y., Nakafuku, M., Yamamori, B., Feng, J., Nakano, T., Okawa, K., Iwamatsu, A., and Kaibuchi, K. (1996). Regulation of myosin phosphatase by Rho and Rho-associated kinase (Rho-kinase). *Science* **273**, 245-248

Kraulis, P. J. (1991). MOLSCRIPT - A program to produce both detailed and schematic plots of protein structures. *J. Appl. Crystallogr.* **24**, 946-950

Krengel, U., Schlichting, L., Scherer, A., Schumann, R., Frech, M., John, J., Kabsch, W., Pai, E. F., and Wittinghofer, A. (1990). Three-dimensional structures of H-ras p21 mutants: molecular basis for their inability to function as signal switch molecules. *Cell* **62**, 539-548

Lambright, D. G., Noel, J. P., Hamm, H. E., and Siglar, P. B. (1994). Structural determinants for activation of the alpha-subunit of a heterotrimeric G protein. *Nature* **369**, 621-628

Laskowski, R. A., MacArthur, M. W., Moss, D. S., and Thornton, J. M. (1993). PROCHECK: a program to check the stereochemical quality of protein structures. *J. Appl. Crystallogr.* **26**, 283-291

Leung, T., Chen, X. Q., Manser, E., and Lim, L. (1996). The p160 RhoA-binding kinase ROK alpha is a member of a kinase family and is involved in the reorganization of the cytoskeleton. *Mol. Cell. Biol.* **16**, 5313-5327

Li, R., and Zheng, Y. (1997). Residues of the Rho family GTPases Rho and Cdc42 that specify sensitivity to Dbl-like guanine nucleotide exchange factors. *J. Biol. Chem.* **272**, 4671-4679

Machesky, L. M., and Hall, A. (1996). Rho: a connection between membrane signalling and the cytoskeleton. *Trends Cell Biol.* **6**, 304-310

Madaule, P., and Axel, R. (1985). A novel ras-related gene family. *Cell* **41**, 31-40

Madaule, P., Furuyashiki, T., Reid, T., Ishizaki, T., Watanabe, G., Morii, N., and Narumiya, S. (1995). A novel partner for the GTP-bound forms of rho and rac. *FEBS. Lett.* **377**, 243-248

Madaule, P., Eda, M., Watanabe, N., Fujisawa, K., Matsuoka, T., Bito, H., Ishizaki, T., and Narumiya, S. (1998). Role of citron kinase as a target of the small GTPase Rho in cytokinesis. *Nature* **394**, 491-494

Manser, E., Leung, T., Salihuddin, H., Tan, L., and Lim, L. (1993). A non-receptor tyrosine kinase that inhibits the GTPase activity of p21cdc42. *Nature* **363**, 364-367

Manser, E., Leung, T., Salihuddin, H., Zhao, Z. S., and Lim, L. (1994). A brain serine /threonine protein kinase activated by Cdc42 and Rac1. *Nature* **367**, 40-46

Marshall, M. S. (1993). The effector interactions of p21ras. *Trends Biochem. Sci.* **18**, 250-254

Matsui, T., Amano, M., Yamamoto, T., Chihara, K., Fukata, Y., Nakafuku, M., Ito, M., Nakano, T., Okawa, K., Iwamatsu, A., and Kaibuchi, K. (1996). Rho-associated kinase, a novel serine/threonine kinase, as a putative target for small GTP binding protein Rho. *EMBO J.* **15**, 2208-2216

Matsui, T., Maeda, M., Doi, Y., Yonemura, S., Amano, M., Kaibuchi, K., Tsukita, S., and Tsukita, S. (1998). Rho-kinase phosphorylates COOH-terminal threonines of ezrin/radixin /moesin (ERM) proteins and regulates their head-to-tail association. *J. Cell Biol.* **140**, 647-657

Matthews, B. W. (1968). Solvent content of protein crystals. *J. Mol. Biol.* **33**, 491-497

Merritt, E. A., and Bacon, D. J. (1997). Raster3d: Photorealistic molecular graphics. *Methods. Enzymol.* **277**, 505-524

Milburn, M. V., Tong, L., de Vos, A. M., Brünger, A., Yamaizumi, Z., Nishimura, S., and Kim, S. H. (1990). Molecular switch for signal transduction: structural differences between active and inactive forms of protooncogenic ras proteins. *Science* **247**, 939-945

Mixon, M. B., Lee, E., Coleman, D. E., Berghuis, A. M., Gilman, A. G., and Sprang, S. R. (1995). Tertiary and quaternary structural changes in Giα1 induced by GTP hydrolysis. *Science* **270**, 954-960

Morii, N., Sekine, A., Ohashi, Y., Nakao, K., Imura, H., Fujiwara, M., and Narumiya, S. (1988). Purification and properties of the cytosolic substrate for botulinum ADP-ribosyltransfer ase. Identification as an Mr 22,000 guanine nucleotide-binding protein. *J. Biol. Chem.* **263**, 12420-12426

Morii, N., Kawano, K., Sekine, A., Yamada, T., and Narumiya, S. (1991). Purification of GTPase-activating protein specific for the rho gene products. *J. Biol. Chem.* **266**, 7646-7650

Narumiya, S. (1996). The small GTPase Rho: cellular functions and signal transduction. *J. Biochem.* **120**, 215-228

Nassar, N., Horn, G., Herrmann, C., Scherer, A., McCormick, F., and Wittinghofer, A. (1995). The 2.2 Å crystal structure of the Ras-binding domain of the serine/threonine kinase c-Raf1 in complex with Rap1A and a GTP analogue. *Nature* **375**, 554-560

Nassar, N., Horn, G., Herrmann, C., Scherer, A., McCormick, F., and Wittinghofer, A. (1996). Ras/Rap effector specificity determined by charge reversal. *Nat. Struct. Biol.* **3**, 723-

Navaza, J. (1994). AMoRe - An automated package for molecular replacement. *Acta Crystallogr. Sec. A* **50**, 157-163

Nicholls, A., Bharadwaj, R., and Honig, B. (1993). GRASP - graphical repressentation and analysis of surface properties. *Biophys. J.* **64**, A166

Nisimoto, Y., Freeman, J. L. R., Motalebi, S. A., Hirshberg, M., and Lambeth, J. D. (1997). Rac binding to p67phox: structural basis for interactions of the Rac1 effector region and insert region with components of the respiratory burst oxidase. *J. Biol. Chem.* **272**, 18834-18841

Noel, J. P., Hamm, H. E., and Sigler, P. B. (1993). The 2.2 Å crystal structure of transducin-alpha complexed with GTPγS. *Nature* **366**, 654-663

Pai, E. F., Krengel, U., Petsko, G. A., Goody, R. S., Kabsch, W., and Wittinghofer, A. (1990). Refined crystal structure of the triphosphate conformation of H-ras p21 at 1.35 Å resolution: implications for the mechanism of GTP hydrolysis. *EMBO J.* **9**, 2351-2359

Perona, R., Montaner, S., Saniger, L., Sanchez, P. I., Bravo, R., and Lacal, J. C. (1997). Activation of the nuclear factor-κB by Rho, CDC42, and Rac-1 proteins. *Genes Dev.* **11**, 463-475

Reid, T., Furuyashiki, T., Ishizaki, T., Watanabe, G., Watanabe, N., Fujisawa, K., Morii, N., Madule, P., and Narumiya, S. (1996). Rhotekin, a new putative target for Rho bearing homology to a serine/threonine kinase, PKN, and rhophilin in the rho-binding domain. *J. Biol. Chem.* **271**, 13556-13560

Ren, X.-D., Bokoch, G. M., Traynor-Kaplan, A., Jenkins, G. H., Anderson, R. A., and Schwartz, M. A. (1996). Physical association of the small GTPase Rho with a 68-kDa phosphatidylinositol 4-phosphate 5-kinase in Swiss 3T3 cells. *Mol. Cell. Biol.* **7**, 435-442

Rittinger, K., Walker, P. A., Eccleston, J. F., Nurmahomed, K., Owen, D., Laue, E., Gamblin, S. J., and Smerdon, S. J. (1997a). Crystal structure of a small G protein in complex with the GTPase-activating protein rhoGAP. *Nature* **388**, 693-697

Rittinger, K., Walker, P. A., Eccleston, J. F., Smerdon, S. J., and Gamblin, S. J. (1997b). Structure at 1.65 Å of RhoA and its GTPase-activating protein in complex with a transition-state analogue. *Nature* **389**, 758-762

Rossmann, M. G., and Blow, D. M. (1962). *Acta Crystallogr.* **15**, 24-31

Scheffzek, K., Klebe, C., Fritz-Wolf, K., Kabsch, W., and Wittinghofer, A. (1995). Crystal structure of the nuclear Ras-related protein Ran in its GDP-bound form. *Nature* **374**, 378-381

Schlichting, I., Almo, S., Rapp, G., Wilson, K., Petratos, K., Lentfer, A., Wittinghofer, A., Kabsch, W., Pai, E. F., Petsko, G. A., and Goody, R. S. (1990). Time-resolved X-ray crystallographic study of the conformational change in Ha-Ras p21 protein on GTP hydrolysis. *Nature* **345**, 309-315

Schmidt, G., Sehr, P., Wilm, M., Selzer, J., Mann, M., and Aktories, K. (1997). Gln 63 of Rho is deamidated by Escherichia coli cytotoxic necrotizing factor-1. *Nature* **387**, 725-729

Sekine, A., Fujiwara, M., and Narumiya, S. (1989). Asparagine residue in the rho gene product is the modification site for botulinum ADP-ribosyltransferase. *J. Biol. Chem.* **264**, 8602-8605

Self, A. J., Paterson, H. F., and Hall, A. (1993). Different structural organization of Ras and Rho effector domains. *Oncogene* **8**, 655-661

Symons, M. (1996). Rho family GTPases: the cytoskeleton and beyond. *Trends Biochem. Sci.* **21**, 178-181

Takai, Y., Sasaki, T., Tanaka, K., and Nakanishi, H. (1995). Rho as a regulator of the cytoskeleton. *Trends Biochem. Sci.* **20**, 227-231

Tan, J. L., Ravid, S., and Spudich, J. A. (1992). Control of nonmuscle myosins by phosphorylation. *Annu. Rev. Biochem.* **61**, 721-759

Tominaga, T., Ishizaki, T., Narumiya, S., and Barber, D. L. (1998). p160ROCK mediates RhoA activation of Na-H exchange. *EMBO J.* **17**, 4712-4722

Tong, L., de Vos, A. M., Milburn, M. V., and Kim, S. H. (1991). Crystal structures at 2.2 Å resolution of the catalytic domains of normal ras protein and an oncogenic mutant complexed with GDP. *J. Mol. Biol.* **217**, 503-516

Van Aelst, L., and D'Souza-Schorey, C. (1997) Rho GTPases and signaling networks. *Genes Dev.* **11**, 2295-2322

Watanabe, G., Saito, Y., Madule, P., Ishizaki, T., Fujisawa, K., Morii, N., Mukai, H., Ono, Y., Kakizuka, A., and Narumiya, S. (1996). Protein kinase N (PKN) and PKN-related protein rhophilin as targets of small GTPase Rho. *Science* **271**, 645-648

Watanabe, N., Madule, P., Reid, T., Ishizaki, T., Watanabe, G., Kakizuka, A., Saito, Y., Nakao, K., Hockusch, B. M., and Narumiya, S. (1997). p140mDia, a mammalian homolog of *Drosophila* diaphanous, is a target protein for Rho small GTPase and is a ligand for profilin. *EMBO J.* **16**, 3044-3056

Wei, Y., Zhang, Y., Derewenda, U., Liu, X., Minor, W., Nakamoto, R. K., Somlyo, A. V., Somlyo, A. P., and Derewenda, Z. S. (1997). Crystal structure of RhoA-GDP and its functional implications. *Nat. Struct. Biol.* **4**, 699-703

Wittinghofer, A., and Nassar, N. (1996). How Ras-related proteins talk to their effectors. *Trends Biochem. Sci.* **21**, 488-491

Wu, W. J., Leonard, D. A., Cerione, R. A., and Manor, D. (1997). Interaction between Cdc42Hs and RhoGDI is mediated through the Rho insert region. *J. Biol. Chem.* **272**, 26153-26158

Wu, W. J., Lin, R., Cerione, R. A., and Manor, D. (1998). Transformation activity of Cdc42 requires a region unique to Rho-related proteins. *J. Biol. Chem.* **273**, 16655-16658

Yaku, H., Sasaki, T., and Takai, Y. (1994). The Dbl oncogene product as a GDP/GTP exchange protein for the Rho family: its properties in comparison with those of Smg GDS. *Biochem. Biophys. Res. Commun.* **198**, 811-817

Yamamoto, K., Kondo, J., Hishida, T., Teranishi, Y., and Takai, Y. (1988). Purification and characterization of a GTP-binding protein with a molecular weight of 20,000 in bovine brain membranes. Identification as the rho gene product. *J. Biol. Chem.* **263**, 9926-9932

Zheng, Y., Olson, M. F., Hall, A., Cerione, R. A., and Toksoz, D. (1995). Direct involvement of the small GTP-binding protein Rho in lbc oncogene function. *J. Biol. Chem.* **270**, 9031-9034